



HAL
open science

Experimental implementation of a finite-time controller for the axisymmetric vibration modes of a tom-tom drum

Marc Wijnand, Brigitte d'Andréa-Novel, Thomas Hélie, David Roze

► **To cite this version:**

Marc Wijnand, Brigitte d'Andréa-Novel, Thomas Hélie, David Roze. Experimental implementation of a finite-time controller for the axisymmetric vibration modes of a tom-tom drum. 2024. hal-04442381

HAL Id: hal-04442381

<https://hal.science/hal-04442381>

Preprint submitted on 6 Feb 2024

HAL is a multi-disciplinary open access archive for the deposit and dissemination of scientific research documents, whether they are published or not. The documents may come from teaching and research institutions in France or abroad, or from public or private research centers.

L'archive ouverte pluridisciplinaire **HAL**, est destinée au dépôt et à la diffusion de documents scientifiques de niveau recherche, publiés ou non, émanant des établissements d'enseignement et de recherche français ou étrangers, des laboratoires publics ou privés.



Distributed under a Creative Commons Attribution 4.0 International License

Experimental implementation of a finite-time controller for the axisymmetric vibration modes of a tom-tom drum

 Marc Wijnand^{1,*},  Brigitte d'Andréa-Novel¹,  Thomas Hélie², and  David Roze²

S₃AM team, STMS Lab (IRCAM – ²CNRS – ¹Sorbonne Université), Paris, France

* marc.wijnand@ircam.fr

This paper is concerned with the experimental implementation of a previously derived finite-time observer-regulator controlling the current of a loudspeaker mounted in a tom-tom drum, based on the measurement of its cavity pressure. The control goal is to modify frequency and damping of the axisymmetric vibration modes of the tom-tom membrane, by modifying the cavity volume.

The first contribution constitutes the identification of the physical parameters of the tom-tom drum, such as membrane tension (from the frequencies of its observed Chladni figures) and viscous damping coefficient.

Secondly, the testbench for the controller evaluation is developed. It is shown how a reproducible excitation with a drumstick can be achieved. Then, the control law is implemented on a microcontroller (Coala). A chattering phenomenon is observed, caused by the numerical stiffness of the finite-time control law, that can be removed by applying a regularization based on a local softening linear interpolation close to the origin.

Finally, it is shown that the controller is able to modify frequencies of the axisymmetric vibration modes of the tom-tom membrane. However, because of the disparity between model and measurements, it is difficult to quantify the controller performance in achieving a prescribed frequency shift. It is proposed to refine the model, in particular by taking into account the sound propagation inside the cavity.

This work is an extension of [Wijnand 2021, Chapter 10; Wijnand et al. 2023].

Keywords musical acoustics, active control of musical instruments, finite-time control, membranophones, experimental validation

1 Introduction

1.1 Active control of musical instruments

Active control [Elliott et al. 1993; Fuller et al. 1996] of musical instruments consists in adding a control loop to an existing acoustic musical instrument that is being played by a musician [Besnainou 1999; Besnainou 2006; Berdahl et al. 2007]. In terms of the actuator type, two classes of active vibration control are distinguished. In the case of *acoustical active control*, the control acts on a fluid medium. An example is the use of a loudspeaker to create destructive interference in order to cancel sound. In the case of *structural active control*, the control acts on a solid. One can for example attach an actuator to the soundboard of a violin.

In most cases of active control of musical instruments, the goal is not to reduce vibrations as much as possible, but to change frequencies or damping coefficients of the instrument's vibration, enabling the musician to enlarge his sound palette while keeping the ergonomics of the original instrument. One can mention for instance applications to the (violin/guitar) string [Berdahl et al. 2006; Benacchio et al. 2015; Wijnand et al. 2022], (xylophone) beam [Boutin et al. 2015], (clarinet) tube [Meurisse et al. 2015a], (Chinese gong) metal plate [Jossic et al. 2017].

Furthermore, active control of musical instruments can be invoked for the study of their dynamical behaviour [Benacchio et al. 2016], or for the removal of unwanted phenomena such as the so-called wolf note of the cello [Neubauer et al. 2018], or the bad playability of certain notes on the trombone when using a straight mute [Meurisse et al. 2015b].

1.2 Membranophones

There exist a great variety of percussion instruments that are membranophones, whose sound is essentially produced by a membrane, some examples of which are shown in Fig. 1. They can be categorized [Von Hornbostel et al. 1914] according to the excitation mechanism by the musician, and by the form of the cavity containing a volume of air, if present. Because of the coupling between membrane and air in a cavity, the harmonicity of the axisymmetric vibration modes of the membrane is improved [Christian et al. 1984], and the acoustical efficiency of the instrument increased [Chaigne et al. 2016].

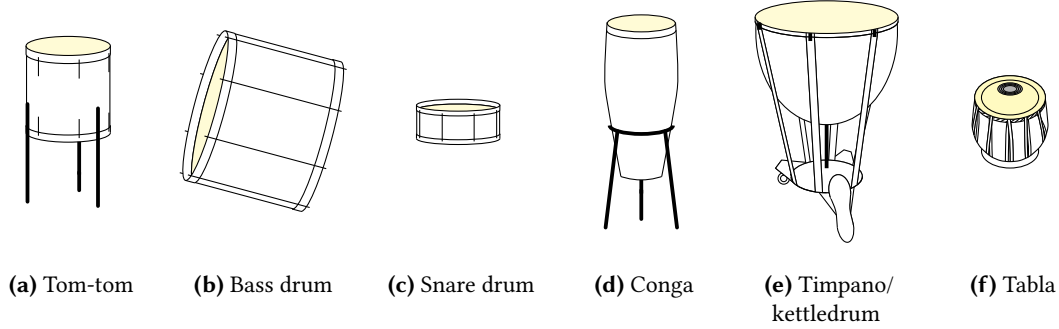


Figure 1: Examples of membranophones coupling a membrane to a cavity (after [Michels 1988; Berg et al. 2005]).

1.2.1 The tom-tom drum

The tom-tom drum is a directly struck membranophone. It consists of a cylindrical body with a top (*batter head*) and bottom (*resonant head*) membrane and is a standard part of a drum kit (containing two rack toms and the bigger floor tom or low tom). The sound of the tom-tom drum is referred to as "indeterminately pitched" or "having a less clear pitch" [Solomon 2016], putting it in an ambiguous position between pitched instruments (such as the timpano, Fig. 1(e)) and unpitched instruments (such as the bass drum, Fig. 1(b)).

1.2.2 Vibration of the circular membrane

Some elements of the vibration of the circular membrane are indicated here. More details on inharmonicity, air charge [Fletcher et al. 2012, Chapter 18] and damping are given in [Wijnand 2021, §9.2].

Circular membrane attached at its rim The transverse vibration of the circular membrane in a vacuum attached at its rim is described by the wave equation [Kinsler et al. 1999, §4.2; Graff 2012], whose spatial eigenfunctions are

$$\begin{cases} \Psi(r, \theta) = J_n(\lambda_{nm}r) \cos n\theta \\ \hat{\Psi}(r, \theta) = J_n(\lambda_{nm}r) \sin n\theta, \end{cases} \quad (1)$$

with $J_n(\cdot)$ Bessel functions of the first kind of order n and wave numbers λ_{nm} are obtained as the solution of $J_n(\lambda_{nm}a) = 0$, a being the radius of the circular membrane. The first eigenmodes are drawn in Fig. 2. One observes that modes with $n = 0$ are axisymmetric (w.r.t. the axis perpendicular through the membrane at rest, at its middle), and modes with (integer) $n > 0$ are not axisymmetric.

Coupling to cavity When a circular membrane attached at its rim is coupled to a volume of air V_0 , its axisymmetric modes will cause a net volume change, that is expressed as a pressure term in the wave equation. As opposed to the case of the membrane without cavity (1), the axisymmetric modes become [Morse 1995]

$$\Phi(r, \theta) = [J_0(\lambda_m r) - J_0(\lambda_m a)], \quad (2)$$

where the wave numbers λ_m satisfy the characteristic equation

$$\lambda_m^2 a^2 J_0(\lambda_m a) = -B J_2(\lambda_m a) \text{ with } B \triangleq \frac{\pi a^4 \gamma p_0}{TV_0}, \quad (3)$$

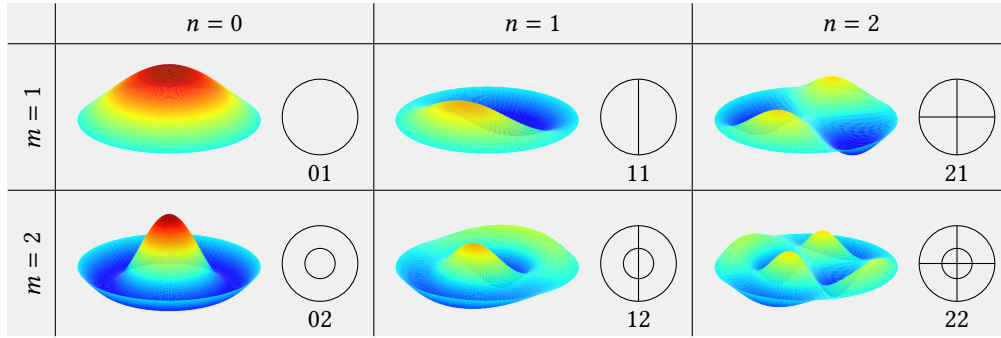


Figure 2: A few eigenmodes $\Psi_{nm}(r, \theta)$ for the circular membrane attached at its rim. The diagrams show the nodal circles and lines: the locus that remains motionless for the given eigenmode nm , and that can be visualized experimentally as a Chladni figure.

and where the dimensionless quantity B can be interpreted as the ratio of the restoring force applied by the air in the cavity to the membrane tension [Kinsler et al. 1999].

Deviations of the linear model In practice, experimentally observed modes often deviate from the linear model (1)-(2) due to several phenomena.

- **Non-uniform density** Some instruments, such as the Indian *tabla* [Sathej et al. 2009; Maugeais 2014; Samejima et al. 2016] and *mridanga* and the Myanmar *pat wain* [Bader 2016], have a non-uniform surface mass density due to applied paste, that can be used for tuning.
- **Non-uniform tension** Depending on the tuning mechanism (6 tension rods in the case of a tom-tom drum), the tension can vary more or less along the circumference of the membrane [Samejima et al. 2016]. This can cause a frequency difference between two spatial eigenfunctions $\Psi_{nm}(r, \theta)$ and $\tilde{\Psi}_{nm}(r, \theta)$ that theoretically have the same eigenfrequency (*peak doubling* or *mode splitting*). In [Worland 2010] for instance, frequency differences of 2 – 28 Hz were measured in a tom-tom drum.

Furthermore, variation in tension can modify the shape of the modes ([Anderson 1978], observed using interferometry in [Worland 2010], Fig. 3).

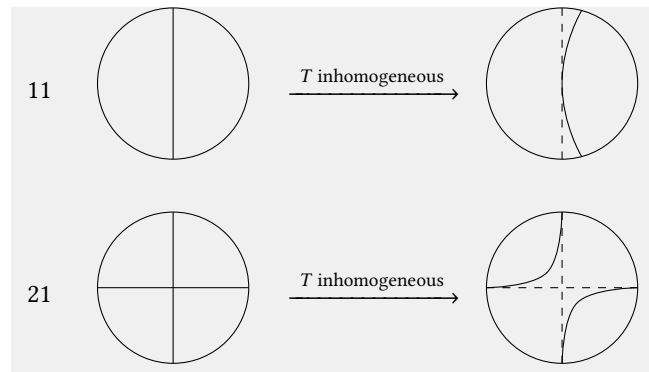


Figure 3: Two examples of deformations of modes due to inhomogeneous tension.

- **Tension modulation (pitch glide)** High excitation amplitudes lead to a tension increase, leading to a pitch glide phenomenon with higher eigenfrequencies that descend to their values corresponding to the linear regime [Rossing 1982a; Richardson 2010, §2.2.7; Torin et al. 2014]. This phenomenon is easier to obtain when the membrane was tuned to a low tension [Richardson 2010, §2.2.7].

For the case of a tom-tom drum with a diameter of 32 – 33 cm, an increase in frequency of 8 – 10% (more than a semitone) has been reported in [Bork 1983; Rose 1978]. In [Dahl 1997], one mentions a pitch glide of even 20 Hz (almost 4 semitones) for the fundamental when hitting hard on a tom-tom drum, and it is argued that for the perception of this instrument, this phenomenon could partially be masked by the presence of high-frequency components. In [Cahoon 1970; Fletcher et al. 1978], the case of a bass drum is considered,

where frequency changes of 6 – 10% are reported when hitting hard (ca. 3.5 Hz or a semitone, for the case of a typical transverse displacement of 6 mm).

1.3 Active control of membranophones

Active control has been applied to following percussion instruments with a membrane-cavity coupling. In [Rollow IV 2003], PID and stabilizing feedforward modal controllers for a *drumhead* were developed, using four accelerometers on the drumhead as sensors and four loudspeakers acting on the cavity as actuators. Experimentally, a suppression of one membrane mode was obtained, yet no frequency shift. A *bass drum* [Lupone et al. 2005] was controlled by a negative feedback, using a piezoceramic sensor attached to the rim to measure the membrane deflection and a single loudspeaker as actuator. A *conga* [Van Walstijn et al. 2005] was endowed with a contact microphone attached to the membrane as sensor and a single loudspeaker used as actuator enables to modify the instrument’s frequency response. Feedback of a piezoelectric sensor placed on the batter head of a *tom-tom drum* [Gregorio et al. 2018] was applied on the resonant head by an electromagnetic actuator. A pickup dynamic microphone was placed inside an electromagnetic actuator placed on the batter head of a *bass drum* in [Rector et al. 2014]. Recently, a *snare drum* [Williams et al. 2020] was controlled using an optical sensor on the batter head, and multiple actuators: two electrodynamic tactile transducers on the resonant head, and an additional loudspeaker on a frame mounted inside the cavity.

The contribution of this paper focuses on the use of ODE finite-time control methods [Bhat et al. 2000], offering advantages regarding time constraints (faster convergence than an asymptotic control law) and robustness, but being necessarily non Lipschitz continuous at the origin [Haimo 1986; Moulay et al. 2006] (which can cause numerical problems). Furthermore, in the described setup, neither the sensor nor the actuator are in the domain of the controlled membrane.

1.4 Article structure

In Section 2, the previously obtained model and controller are restated. The physical constants that they contain are identified in Section 3. Then, a testbench is constructed (Section 4) and the obtained results are evaluated (Section 5).

2 Theoretical results

This section review the model and controller that were obtained in [Wijnand et al. 2019; Wijnand et al. 2020].

2.1 Model

The coupled PDE-ODE physical model for the tom-tom drum consisting of the top membrane coupled to the cavity and loudspeaker as depicted in Figure 4 is presented in Section 2.1.1. In Section 2.1.2, an ODE state-space reformulation is obtained after projection on the spatial eigenmodes of the membrane coupled to the cavity.

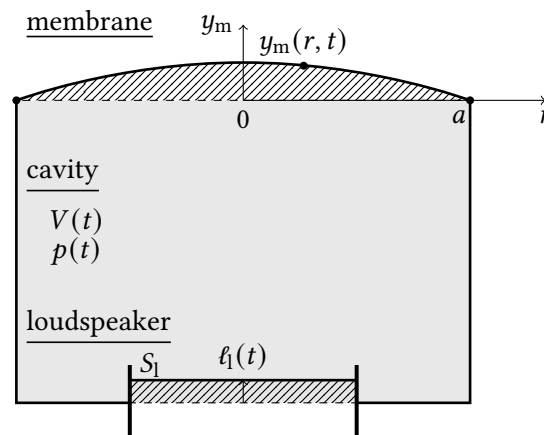


Figure 4: Geometry of the system.

2.1.1 Physical model

Following coupled PDE-ODE model for the system shown in Fig. 4 was obtained:

$$\begin{cases} T\Delta y_m(r, t) + p_c(t) = \sigma_m \frac{\partial^2}{\partial t^2} y_m(r, t) + \mu \frac{\partial}{\partial t} y_m(r, t) \\ p_c(t) = -\gamma \frac{p_0}{V_0} \left[\int_{\mathcal{S}} y_m(r, t) \, d\mathcal{S}(r) - S_l \ell_1(t) \right] \\ m_l \ddot{\ell}_1(t) + c_l \dot{\ell}_1(t) + k_l \ell_1(t) = S_l p_c(t) + Bl i_1(t). \end{cases} \quad (4)$$

This model describes the evolutions of the transverse displacement of the tom-tom membrane $y_m(r, t)$, the acoustic pressure in the cavity $p_c(t)$ and the transverse position of the loudspeaker membrane $\ell_1(t)$.

The surface of the membrane \mathcal{S} is defined between $r = 0$ and $r = a$. The membrane is clamped at its rim: $y_m(a, t) = 0$. In polar coordinates, $\Delta = \frac{\partial^2}{\partial r^2} + \frac{1}{r} \frac{\partial}{\partial r}$. The physical constants of the membrane are its tension T , equivalent areal density $\sigma_m = \sigma + 0.85a\rho_{\text{air}}$ (with σ the real areal density, a the membrane's radius and ρ_{air} the volumetric density of air, [Kinsler et al. 1999]), and viscosity coefficient μ . The physical constants of the cavity are the heat capacity ratio of air γ and its pressure p_0 and volume V_0 at rest, that relate the acoustic values (p_c, V_c) to the total values (p, V):

$$\begin{cases} p_c(t) = p(t) - p_0 \\ V_c(t) = V(t) - V_0. \end{cases}$$

The physical constants of the loudspeaker are its surface S_l , the Lorentz force factor Bl (with the length of the loudspeaker coil l inside the magnetic field B), and equivalent mass m_l , damper c_l and spring k_l .

2.1.2 Projection and state-space reformulation

The model (4) is spatially discretized by a modal projection and truncation:

$$y_m(r, t) \approx \sum_{n=1}^N \varphi_n(r) z_n(t),$$

where $z_n(t)$ are the temporal evolutions corresponding to the respective N axisymmetric eigenfunctions of the circular membrane clamped at its rim and coupled to a cavity,

$$\varphi_n(r) = w_n [J_0(\lambda_n r) - J_0(\lambda_n a)],$$

equal to Eq. (2) multiplied by arbitrary weights w_n and with wave numbers λ_n as solutions of the condition (3).

2.2 Control design

A controller for the loudspeaker current is designed, to let its membrane position (and thus the pressure inside the cavity) track in finite time [Bernuau et al. 2015] a reference that realizes a pole placement on the tom-tom membrane, based on the measurement of the cavity pressure only (schematized in Fig. 5). Thus, a modal control of frequencies and/or damping coefficients of the tom-tom membrane is possible.

The obtained finite-time control law reads

$$i_1(t) = \frac{1}{Bl} \left[S_l p_c^m(t) + k_1 \ell_1^m(t) + c_1 \dot{\ell}_1^m(t) - k_3 (\ell_1^m(t) - \ell_1^*(t)) - k_4 (\dot{\ell}_1^m(t) - \dot{\ell}_1^*(t)) - k_1 [\ell_1^m(t) - \ell_1^*(t)]^{\frac{\alpha}{2-\alpha}} - k_2 [\dot{\ell}_1^m(t) - \dot{\ell}_1^*(t)]^\alpha \right], \quad (5)$$

with control parameters $k_1, k_2 > 0$, $\alpha \in]0, 1[$ (to be tuned in simulation [Wijnand et al. 2020]), $k_3 > k_1$, $k_4 > c_1$, and $[x]^\xi \triangleq \text{sgn}(x)|x|^\xi$.

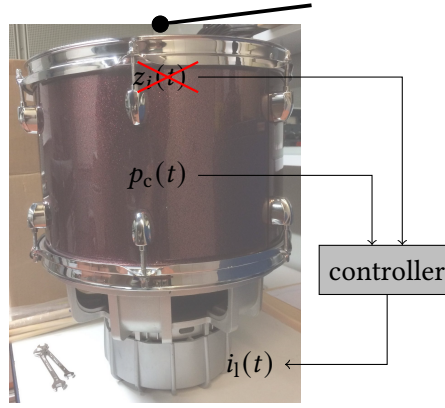


Figure 5: Structure of the controller (observer-regulator): a control law for the loudspeaker current $i_1(t)$ is calculated, based on a measurement of the cavity pressure $p_c^m(t)$ and on an estimation of the temporal evolutions $z_i(t)$ of the first N membrane modes, that are not measured.

The following signals are defined. The real pressure $p_c^m(t)$ is measured by a sensor. The reference pressure is

$$p_c^*(t) \triangleq - \sum_{i=1}^N [k_{i,a} z_i(t) + k_{i,b} \dot{z}_i(t)], \quad (6)$$

where coefficients $k_{i,a}$ and $k_{i,b}$ are chosen to obtain a pole placement that enables to modify modal frequencies and/or damping coefficients of the tom-tom membrane [Wijnand et al. 2020]. The temporal evolutions $z_i(t)$ of the first N membrane modes are estimated by a finite-time observer obtained in [Wijnand et al. 2020, Lemma 2] (after [Perruquetti et al. 2008]). Lastly, the real (resp. reference) loudspeaker position $\ell_1^m(t)$ (resp. $\ell_1^*(t)$) are expressed as function of the real (resp. reference) pressure $p_c^m(t)$ (resp. $p_c^*(t)$), and $z_i(t)$ using relation [Wijnand et al. 2020, Eq. 13]; and similarly for their time derivatives.

3 Identification

In Section 4, a testbench for the controlled tom-tom drum¹ will be built. In order for the microcontroller to be able to calculate the control law (5), the physical parameters listed in Table 1 need to be estimated. The identification methods used for the cavity (Section 3.1), loudspeaker (Section 3.2) and membrane (Section 3.3) are specified below. The references of the used devices are given in Appendix A.

3.1 Cavity

3.1.1 Volume at rest V_0

The volume V_0 of the cavity at rest is estimated from the geometry.

3.2 Loudspeaker

A subwoofer loudspeaker² with nominal exterior diameter of 320 mm is mounted, whose linear parameters are identified experimentally.

3.2.1 Equivalent surface S_1

The equivalent surface S_1 of the membrane is estimated from the geometry.

3.2.2 Thiele & Small parameters (m_1, c_1, k_1, Bl, R, L)

Linear Thiele & Small model Figure 6 shows a schematic representation of an electrodynamic loudspeaker. It is an electro-magneto-mechano-acoustical converter. A modulated electrical tension is applied to its terminals, causing a current to flow in the electrical circuit containing a coil mounted on a moving equipment. This coil is embedded in the magnetic field of a permanent

¹ Model: tom 1309T, Pearl drums, Japan, <https://pearldrums.com>

² Model: AXX 1212, Raveland, US. A datasheet can be found in [Wijnand 2021, Section D.4].

Table 1: List of physical parameters to be estimated.

membrane	a	radius	m
	σ	mass density	$\frac{\text{kg}}{\text{m}^2}$
	T	tension	$\frac{\text{N}}{\text{m}}$
	μ	viscosity coefficient	$\frac{1}{\text{s}}$
cavity	V_0	volume at rest	m^3
loudspeaker	m_1	equivalent mass	kg
	c_1	equivalent damping	$\frac{\text{kg}}{\text{s}}$
	k_1	equivalent stiffness	$\frac{\text{N}}{\text{m}}$
	Bl	Lorentz force factor	$\text{T} \cdot \text{m} = \frac{\text{N}}{\text{A}}$
	R	electrical resistance	Ω
	L	electrical inductance	H
	S_1	equivalent surface	m^2

magnet, so a Laplace/Lorentz force is created on the moving equipment, causing the membrane to move and creating a sound wave.

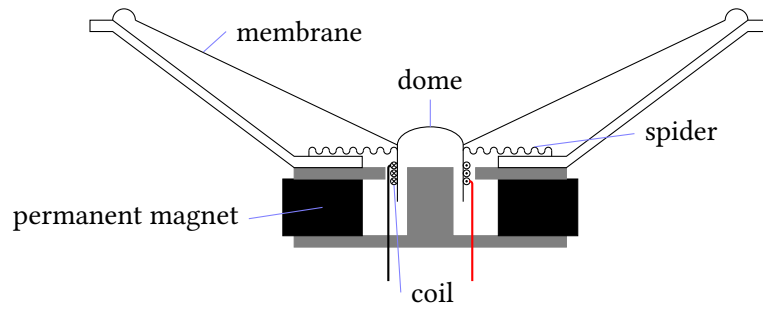


Figure 6: Structure of an electrodynamic loudspeaker.

The linear Thiele & Small model [Thiele 1971a; Thiele 1971b; Small 1972; Small 1973] for the electrodynamic loudspeaker is used, that neglects the spatial modes of the membrane movement, replacing the membrane by a plane piston (here of vertical position $x_1(t)$). The model consists of the force balance on the membrane³,

$$m_1 \ddot{x}_1(t) + c_1 \dot{x}_1(t) + k_1 x_1(t) = Bl i_1(t), \quad (7)$$

completed by the sum of electrical tensions in the equivalent electrical circuit,

$$v_1(t) = R i_1(t) + L \frac{d}{dt} i_1(t) + Bl \dot{x}_1(t), \quad (8)$$

where $v_1(t)$ is the electrical tension applied to the loudspeaker terminals, and R and L respectively the resistance and inductance of the electrical circuit.

There exist several methods for the identification of the Thiele & Small model. For the linear model, as shown above, one has methods in the time [Knudsen et al. 1989] or frequency domain [Klippel et al. 2001]. For the case of nonlinear parameters, we refer the reader to [Brunet 2014; Bouvier 2018; Lebrun 2019]. Moreover, the loudspeaker characteristics can vary as function of temperature [Krump 1997], which is why (online) [Pedersen et al. 2007] identification methods have been developed, capable of tracking the evolution of the characteristics, for use in advanced loudspeaker control algorithms.

³ This equation does not include the influence of a cavity, since the identification is performed without the top membrane.

Frequential identification method for the linear Thiele & Small parameters In the current work, an *offline* standard linear method using the frequency domain is used. A testbench from [Lebrun 2019] is used (Fig. 7), where the loudspeaker is driven with a sine sweep voltage signal $v_1(t) = A \cos(2\pi \int_0^t f(\tau) d\tau)$, where the frequency $f(t)$ increases exponentially between 0.1 Hz and 2000 Hz in 10 s, and voltage $v_1(t)$, current $i_1(t)$ and transverse displacement $x_1(t)$ are measured (Fig. 8).

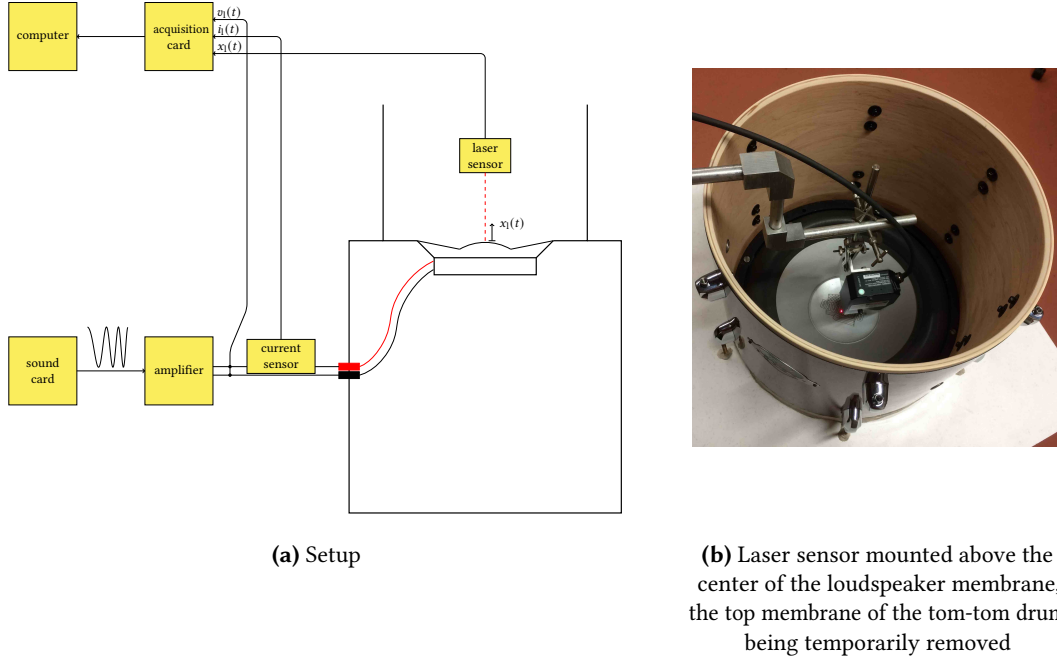


Figure 7: Testbench for loudspeaker identification.

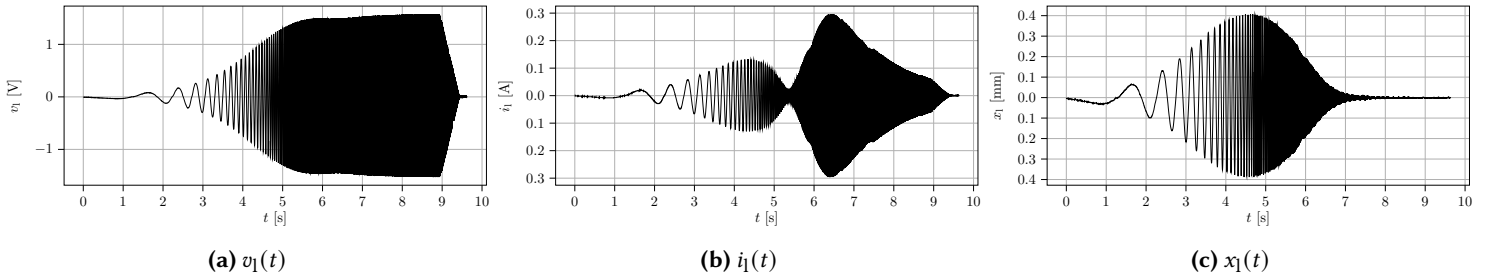


Figure 8: Measurements for the loudspeaker identification.

The physical parameters of the linear Thiele & Small model are obtained by curve fitting the theoretical transfer functions of the linear model (7)-(8),

$$H_{X/I}(s) = \frac{X(s)}{I(s)} = \frac{Bl}{m_1 s^2 + c_1 s + k_1},$$

$$H_{V/I}(s) = \frac{V(s)}{I(s)} = \frac{B^2 l^2 s}{m_1 s^2 + c_1 s + k_1} + Ls + R,$$

$$H_{X/V}(s) = \frac{X(s)}{V(s)} = \frac{Bl}{B^2 l^2 s + (Ls + R)(m_1 s^2 + c_1 s + k_1)},$$

with Laplace transforms

$$\begin{cases} v_1(t) \leftrightarrow V(s), \\ i_1(t) \leftrightarrow I(s), \\ x_1(t) \leftrightarrow X(s), \end{cases}$$

where the Laplace variable s is chosen on the Fourier axis ($s = j\omega = j2\pi f \in j\mathbb{R}$), to the experimentally obtained transfer functions (Fig 9).

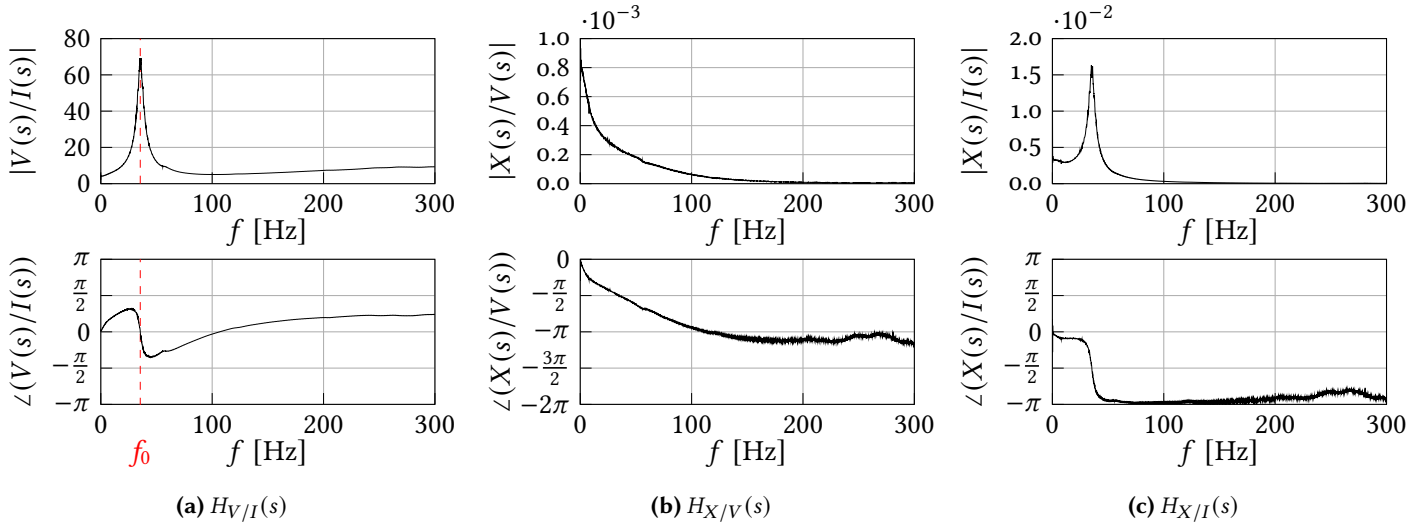


Figure 9: Transfer functions calculated from measurements.

The estimation procedure from [Lebrun 2019] is followed: the mechanical resonance frequency f_0 is obtained from the maximum of $|H_{V/I}(s)|$ (Fig. 9(a)), an initial estimation for the parameters is obtained by curve fitting⁴ $H_{X/I}(s)$ then $H_{V/I}(s)$, used as initial values for a final joint curve fitting of both transfer functions. The resulting estimated transfer function $H_{V/I}(s)$ is shown in Fig. 10.

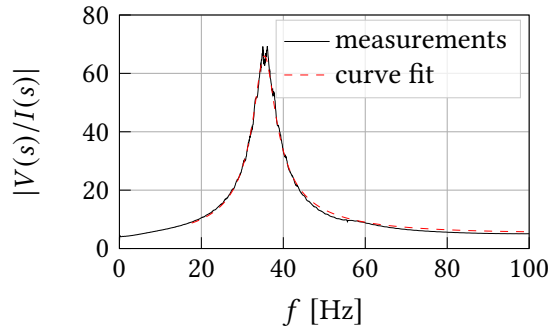


Figure 10: Obtained curve fit: the case of $H_{V/I}(s)$.

3.3 Membrane

A membrane with nominal diameter of 13" (33.0 cm) and 10-mil (0.254 mm) thickness⁵ is mounted on the circular edge of the tom.

3.3.1 Radius a

The effective radius a is estimated from the geometry.

3.3.2 Mass density σ

In the past, membranes were made of skins of animals such as goat [Bertsch 2001] and calf [Harms 2008] for the case of timpani. Nowadays, most membranes are produced in the polyester Mylar[®], that has more homogeneous characteristics, is less sensible to changes in humidity and temperature, and has a greater resistance in traction [Bertsch 2001; Chaigne et al. 2016]. Its surface mass density is about 0.1 kg/m^2 [Chaigne et al. 2016].

The surface mass density of the used tom-tom membrane is obtained by weighing. A very similar value of 0.262 kg/m^2 was found in the same fashion for a timpani membrane in [Rhaouti et al. 1999].

⁴ Curve fitting was done for the interval $[0, 500]$ Hz by a nonlinear numerical method using least squares (*Trust Region Reflective* [Branch et al. 1999]). Note that in [Lebrun 2019], a minimization algorithm is applied to a cost function, weighting the frequencies logarithmically.

⁵ Unknown model by Remo Inc., US, <https://www.remo.com>

3.3.3 Tension T

The tension, which the tom-tom membrane is subjected to, depends on the position of the 6 tuning rods. In the literature, one mentions for instance values between 1000 and 2800 N/m for the case of a tom-tom drum [Samejima et al. 2016] and between 3100 and 3770 N/m for the timpani [Rhaouti et al. 1999]. Furthermore, the spatial nonuniformity of the membrane tension causes mode splitting of the non axisymmetric modes (as mentioned in Section 1.2.2).

Membrane tuning The following tuning method (schematized in Fig. 11 and similar to [Richardson et al. 2010]⁶), is used. A tuning rod is adjusted, the external sound $p_e(t)$ after a strike by an impact hammer at $r \approx \frac{a}{2}$ is recorded (Fig. 12), and the free oscillation (recorded when a zero impact hammer force is measured) is analyzed by FFT⁷ (Fig. 13). Several peaks around 100 Hz (mode 11, see Chladni figures in Fig. 15) are observed. By repeating the procedure, it is tried to let the split versions⁸ of this mode coincide (clearing the drumhead, [Chaigne et al. 2016, Chapter 14]–[Richardson et al. 2010]). In this fashion, a (low) membrane tension is obtained, that is supposed to be as uniform as possible.

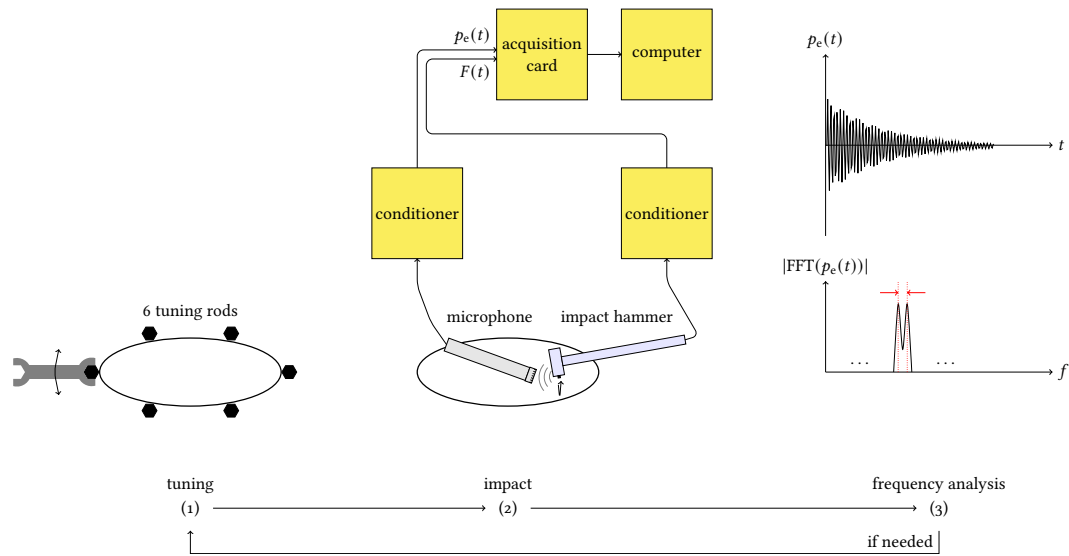


Figure 11: Membrane tuning method.

Estimation methods There exist several methods to estimate the tension T supposed to be uniform for a given tuning, but it is not an easy task. An acoustical method based on the frequency content of the produced sound [Chaigne 2000; Chaigne et al. 2016] will be applied here. A less precise method based on the static deflection of the membrane onto which a mass has been placed [Chaigne 2000; Chaigne et al. 2016] has been applied to a snare drum in [Rossing et al. 1992] and to the described tom-tom drum in [Wijnand 2021, Chapter 10]. A third, even less precise method is based on the moments of the tuning rods [Anderson 1978].

Acoustical estimation method with visualization of Chladni figures In [Chaigne 2000], an estimation method for the membrane tension is described, where the theoretical frequencies of the circular membrane of unknown tension (without cavity and with air charge) are fitted to experimentally observed frequencies in a recorded sound of the struck membrane. In order to apply this method, one needs to clearly identify the frequencies of the first vibration modes of the membrane, which is not a trivial task: as mentioned in Section 1.2.2, the experimentally observed spectra (cf. Fig. 13) can deviate considerably from the linear model (1)-(2). Therefore,

⁶ For more details about different tuning methods, see [Richardson 2010, Chapter 3].

⁷ There exist high resolution methods, allowing for a better resolution than FFT. One can mention frequential methods using interpolation and curve fitting (for example [Sullivan 1997] applied to timpani), temporal methods based on invariance properties of subspaces (such as ESPRIT [Roy et al. 1986; Badeau 2005]), that are used in this paper to estimate the viscosity coefficient μ or the *Snail* [Hélie et al. 2017], that is based on phase demodulation to improve the frequency accuracy.

⁸ (cf. *mode splitting* due to non-uniform tension in Section 1.2.2)

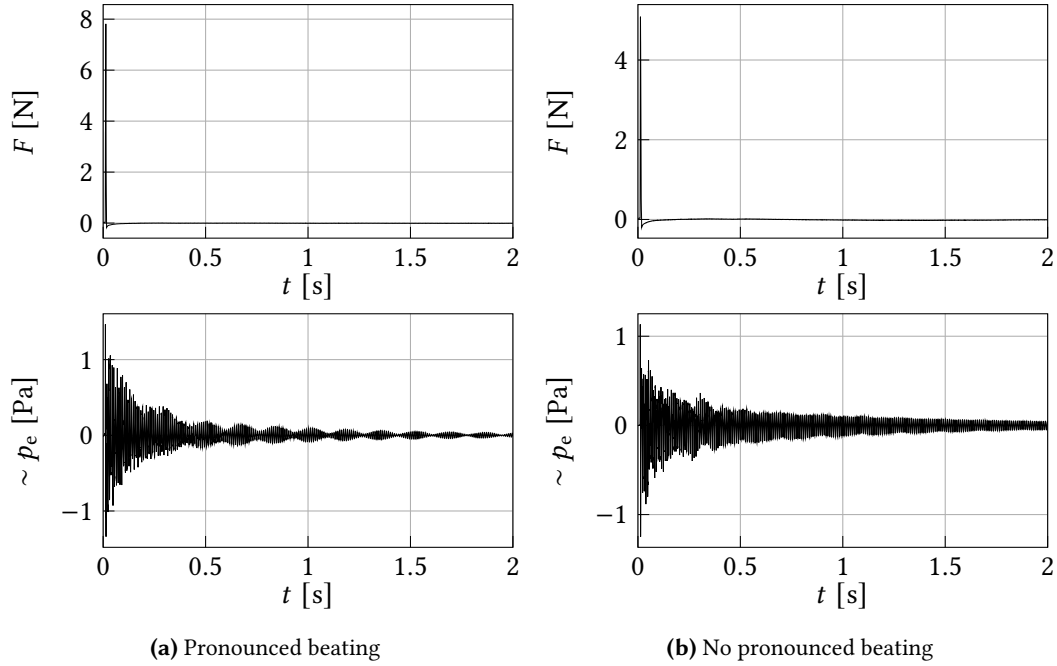
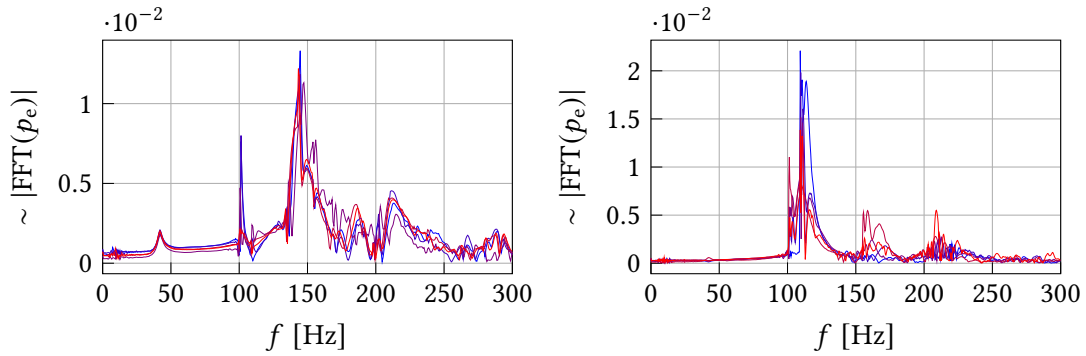


Figure 12: Membrane tuning method: examples of obtained measurements.



(a) Spectra of 5 strikes at $r = 0$ (supposed to correspond to the axisymmetric response). Note the loudspeaker response around 42 Hz **(b)** Spectra of 5 strikes at different points at $r = \frac{a}{2}$

Figure 13: Membrane tuning method: examples of obtained spectra.

we propose to realize Chladni figures of the membrane, in order to distinguish the different vibrational modes⁹. Chladni figures [Chladni 1787] are formed when a structure is set to vibrate at a frequency corresponding to a given eigenmode, and a powder accumulates on stationary zones (circles and lines in the case of the homogeneous circular membrane, cf. Fig. 2). Chladni figures have been obtained for the timpani [Rossing 1982b; Fleischer 2005], tabla [Raman 1934], drumhead [Worland 2011], and the tom-tom drum (upper membrane of a double-membrane tom-tom in [Richardson 2010, Appendix B]). In the current setup, salt was used and the membrane was either excited by the mounted loudspeaker or an additional shaker (see Fig. 14)¹⁰.

The obtained low-frequency Chladni figures are shown in Fig. 15, and some figures at higher frequencies are shown in Appendix B. It is noted that the obtained Chladni figures differ more from the symmetrical theoretical figures than is the case in [Richardson 2010, Appendix B], probably because of a less uniform tuning (cf. Section 1.2.2).

As proposed in [Chaigne 2000], by fitting the theoretical frequencies of the non-axisymmetric

⁹ Alternative methods are for instance the use of a microphone to scan the surface and the display of Lissajous figures obtained by this measurement as function of the membrane excitation [Anderson 1978], or interferometry [Worland 2010].

¹⁰ We note that in [Rossing et al. 1992], sand bags were put against a snare drum in order to damp vibration modes of the walls.

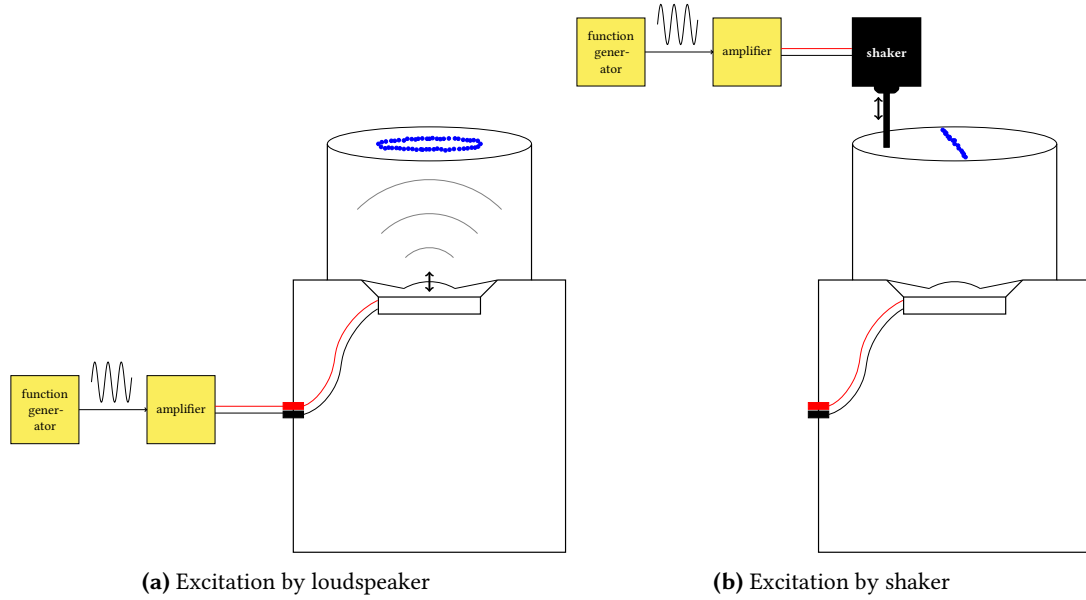


Figure 14: Membrane tension identification: visualisation of Chladni figures.

eigenmodes (that depend on the tension) to the observed frequency ranges for the Chladni figures, the tension can be estimated (Fig. 16).

3.3.4 Viscosity coefficient μ

In our model, the viscosity coefficient μ [1/s] corresponds to the exponential decay of the signal $y_m(r, t)$ in time, that does not depend on frequency. There are several ways to identify this coefficient. In the case of the xylophone bar in [Chaigne et al. 1997] for instance, one excites the structure, stops the excitation, and studies the decaying time of the sound¹¹.

In this paper, the high resolution (HR) ESPRIT (Estimation of Signal Parameters via Rotational Invariance Techniques, [Roy et al. 1986; Badeau 2005]) method is used. The signal to be analyzed $y(t)$ is modeled as a mix of Exponentially Damped Sinusoids (EDS):

$$y(t) = \sum_{q=1}^{\frac{N}{2}} a_q e^{\delta_q t} \cos(2\pi f_q t + \varphi_q). \quad (9)$$

For a given even number N of poles, the ESPRIT method estimates the parameters $(a_q, \delta_q, f_q, \varphi_q)$, by separating the signal $y(t)$ in desired and perturbing contributions, and by using rotational invariance properties in the corresponding subspaces (cf. [Badeau 2005; Le Carrou et al. 2009]). One can set the number of poles N manually, but there also exist methods to estimate the optimal number of poles to represent the given signal $y(t)$ by an EDS model [Badeau 2005, Sec. IV.3-IV.4], such as the ESTER method (ESTimation ERror, [Badeau et al. 2006]).

In order to obtain a physically meaningful estimation for the coefficient μ using the ESPRIT method¹², the signal $y(t)$ (measured external pressure $p_e(t)$) has to cover only the *unforced linear* regime of vibration. This part of the signal to be analyzed is selected by removing the part where the measured excitation force is not zero and by removing the nonlinear dynamic part with a pitch glide, as illustrated in Figures 17–18.

The ESPRIT method is applied to the linear regime of the 5 recordings. The number of poles is increased manually till $N = 8$, which allows for a good fit using 4 low-order modes (example Fig. 19). The mean of the obtained estimations for δ corresponding to mode 02 (around 200 Hz) is taken as estimate for the viscosity coefficient μ .

¹¹ The *matrix pencil* method [Laroche 1993] was used, that is related to the high resolution method that is used below.

¹² In the following, an implementation of the algorithms ESPRIT and ESTER of the toolbox DESAM (Décomposition en Éléments Sonores et Applications Musicales, [Lagrange et al. 2010]) is used.

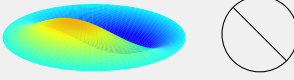





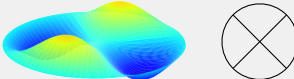


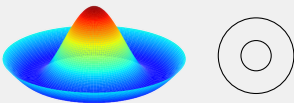



mode	theoretical form	Chladni figures		
11		 105 Hz	 116 Hz	 129 Hz
		 132 Hz	 132 Hz (bis)	
21		 146 Hz (*)	 158 Hz	
02		 201 Hz	 210 Hz	 219 Hz

Figure 15: Obtained low-frequency Chladni figures with corresponding excitation frequencies (*: degenerated form due to non-uniform tension, cf. Fig. 3). During the experiment, the excitation frequency and amplitude were modified until a given mode was obtained. Then, this initial excitation frequency was increased and decreased in order to obtain the frequency ranges at which the same mode is still excited.

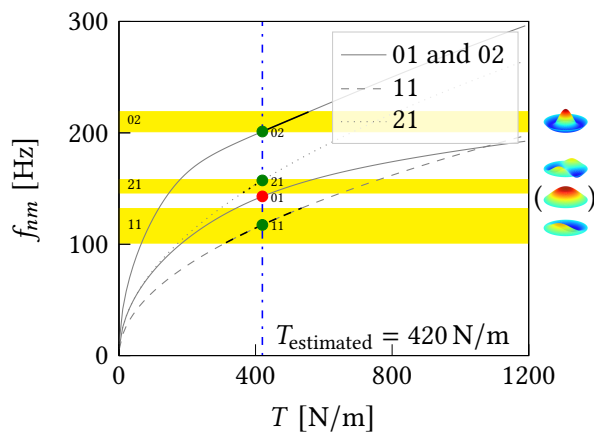


Figure 16: Fit of the frequencies of the model (indicated in gray as function of the unknown tension T) to the frequency ranges of the Chladni figures for modes $nm = 11, 21, 02$ (yellow zones) as observed in Fig. 15.

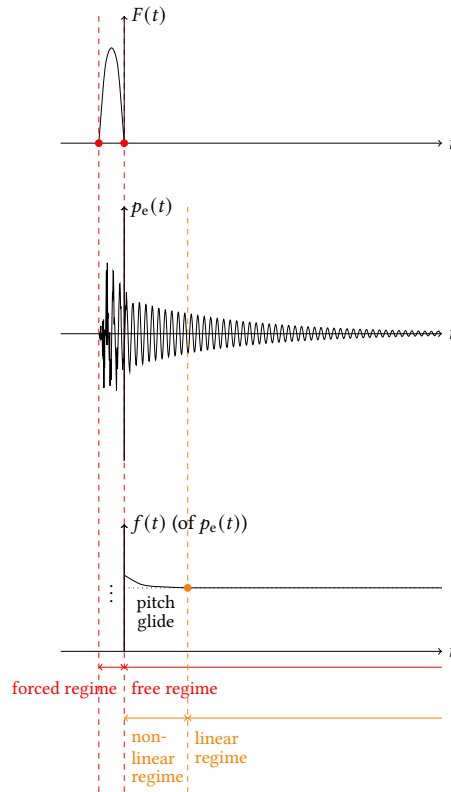
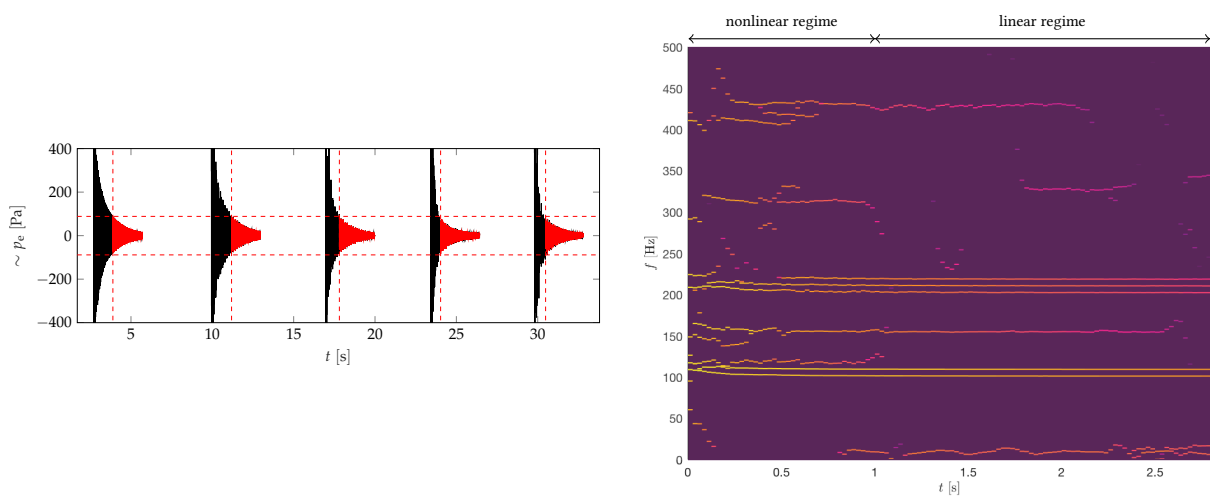


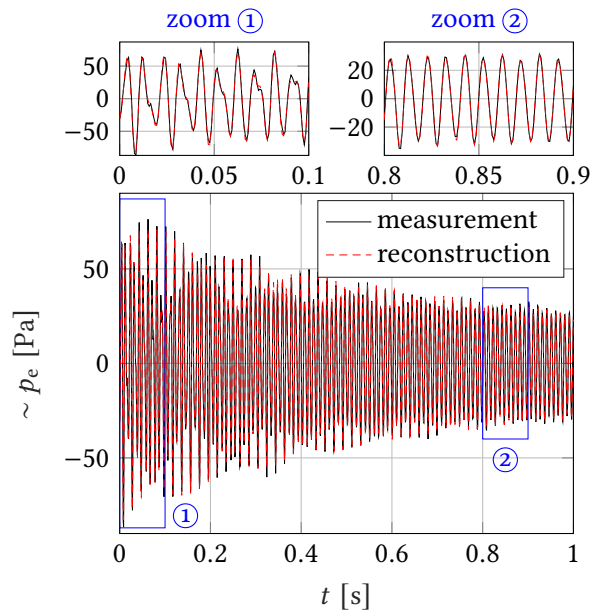
Figure 17: Schematic representation of oscillation regimes in the sound $p_e(t)$ of a strike on the tom-tom membrane with a force $F(t)$. The unforced regime of vibration starts when the excitation force $F(t)$ becomes zero. It consists of a nonlinear dynamic part with a pitch glide in the frequency $f(t)$, followed by a linear dynamic part with a constant frequency.



(a) Temporal signals, the linear regime being indicated in red

(b) HR-ogram ([Lagrange et al. 2010], using the ESPRIT-ESTER method) of one signal. A pitch glide is clearly observed for frequency contributions between 100 and 250 Hz.

Figure 18: Selection of the linear regime in 5 recordings of the struck membrane $p_e(t)$.



(a) Time signals

f_q [Hz]	δ_q [1/s]
101.0621	-0.48282
101.3171	-2.702996
154.9807	-2.946332
202.4544	-1.375677

(b) Corresponding obtained frequencies f_q and damping factors δ_q (see Eq. (9))

Figure 19: Approximation of the measured external pressure $p_e(t)$ by an EDS model with 4 pole pairs by the ESPRIT method: example.

3.4 Conclusion

Table 2 lists the obtained values of the physical parameters¹³.

Table 2: List of identified physical parameters.

membrane	a	radius	0.162	m
	σ	mass density	0.267	$\frac{\text{kg}}{\text{m}^2}$
	T	tension	420	$\frac{\text{N}}{\text{m}}$
	μ	viscosity coefficient	1.4707	$\frac{1}{\text{s}}$
cavity	V_0	volume at rest	0.0195	m^3
loudspeaker	m_1	equivalent mass	0.157	kg
	c_1	equivalent damping	4.87	$\frac{\text{kg}}{\text{s}}$
	k_1	equivalent stiffness	7.80	$\frac{\text{kN}}{\text{m}}$
	Bl	Lorentz force factor	17.4	$\text{T} \cdot \text{m}$
	R	electrical resistance	5.52	Ω
	L	electrical inductance	4.37	mH
	S_1	equivalent surface	0.0515	m^2

4 Testbench

After having identified the physical parameters of the model, the components for the testbench are selected and a reproducible excitation mechanism is built.

4.1 Components

The total setup is shown in Fig. 20. The references of the used devices are given in Appendix A.

- Sensor: the microphone used to measure the pressure inside the cavity $p_c(t)$ is introduced through a vent hole¹⁴ of the drum.
- Actuator: the control law for the current (5) is converted for the voltage-controlled loudspeaker by neglecting its inductance, that is,

$$v_1(t) = Ri_1(t) + L \frac{di_1(t)}{dt} + Bl\dot{h}_1(t) \approx Ri_1(t) + Bl\dot{h}_1(t),$$

as the electric dynamics is faster than the mechanical dynamics in the low-frequency regime. In this fashion, a SISO (single-input-single-output) control loop is obtained.

- Controller: the observer-regulator¹⁵ for $N = 2$ modes is discretized by Euler's explicit method and implemented on a Coala microcontroller, suited for SISO control with a latency lower than 100 μs [Piéchaud 2014]¹⁶.

4.2 Reproducible excitation mechanism

A reproducible excitation mechanism is built by mounting a drumstick in a hinge (Fig. 21(a)), adapting a mallet holder initially developed for the *xiaoluo* gong in [Jossic 2017, Fig. 2.15]. Releasing the drumstick that is initially held against a stop and catching it after one impact, enables to obtain a repeatable force in magnitude and impact point, as shown in Fig. 21.

¹³ Furthermore, the used values for the air are $p_0 = 101\,325\text{ Pa}$, $\rho_{\text{air}} = 1.2\text{ kg/m}^3$, $\gamma = 1.4$.

¹⁴ The vent holes ensure that the pressure inside the cavity at rest equals the atmospheric pressure. In the case of the kettledrum, it has been shown that the presence of a vent hole has little to no influence on the acoustics of the instrument [Rossing 1982b; Chaigne et al. 2016, Chapter 14].

¹⁵ The used observer parameters are ($\theta = 0.86$, $h_1 = 6$, $h_2 = 17.5$, $h_3 = 30$, $h_4 = 33.0625$, $h_5 = 22.125$, $h_6 = 8.125$), and control parameters ($\alpha = 0.9$, $k_1 = 1587$, $k_2 = 14.56$, $k_3 = 2k_1$, $k_4 = 2c_1$).

¹⁶ This microcontroller contains a BeagleBone with Linux and real-time extensions in Xenomai. It can be programmed using Max MSP or (here) C++ code. A sampling period of 100 μs was used, more than a factor 10 [Elliott 2000] bigger than the frequencies of interest, especially the 02 mode around 200 Hz.

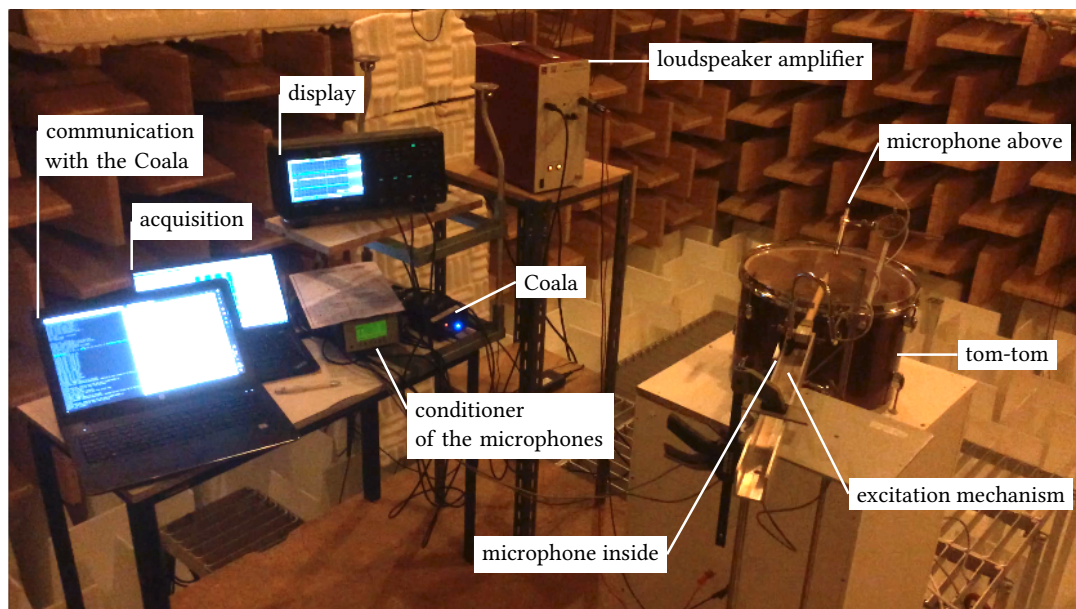
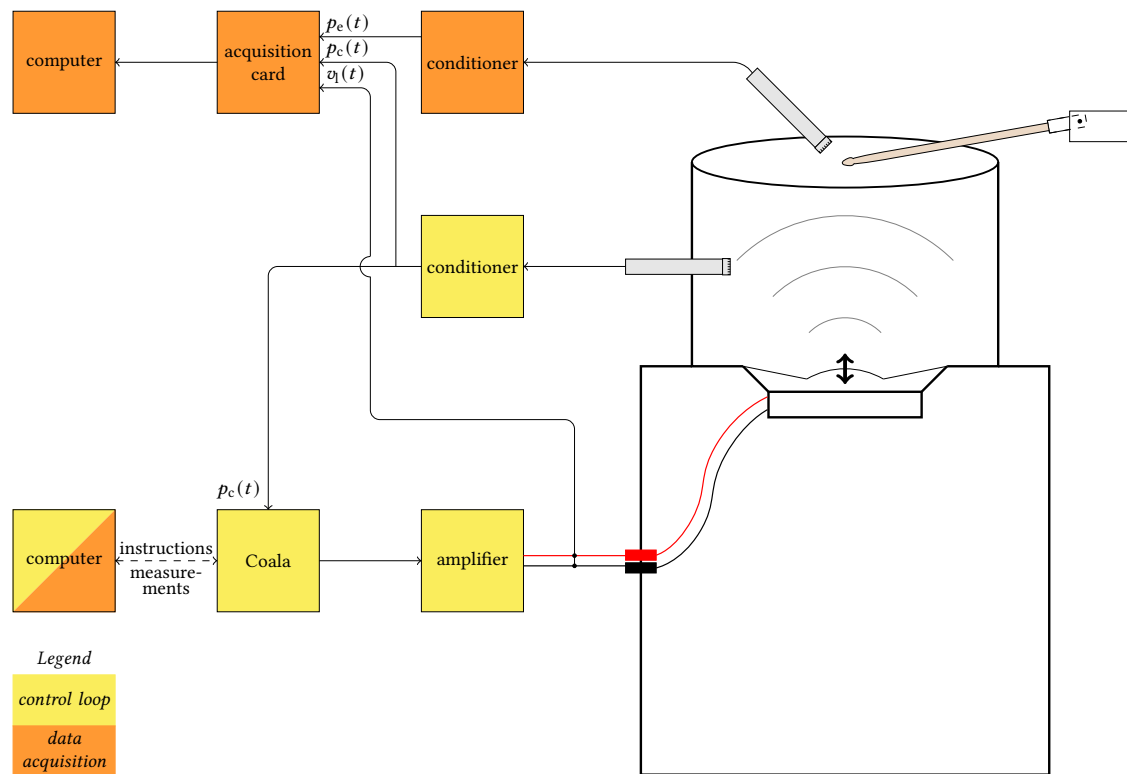
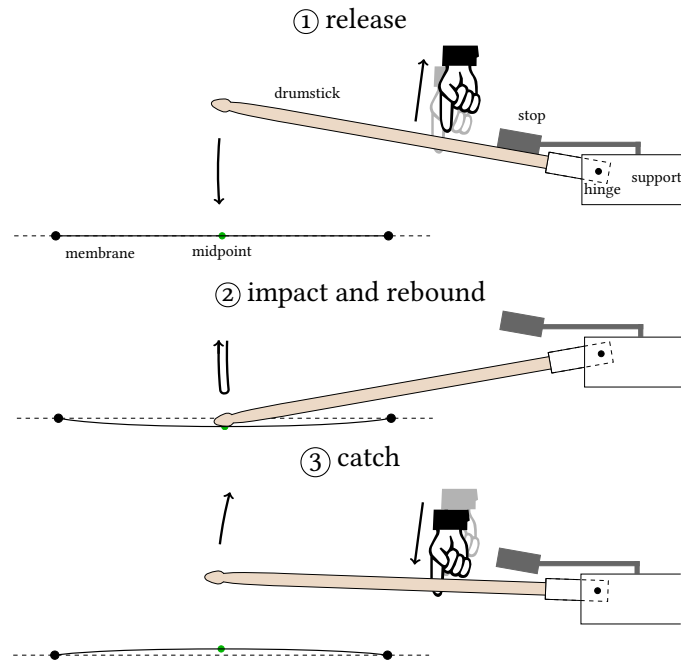
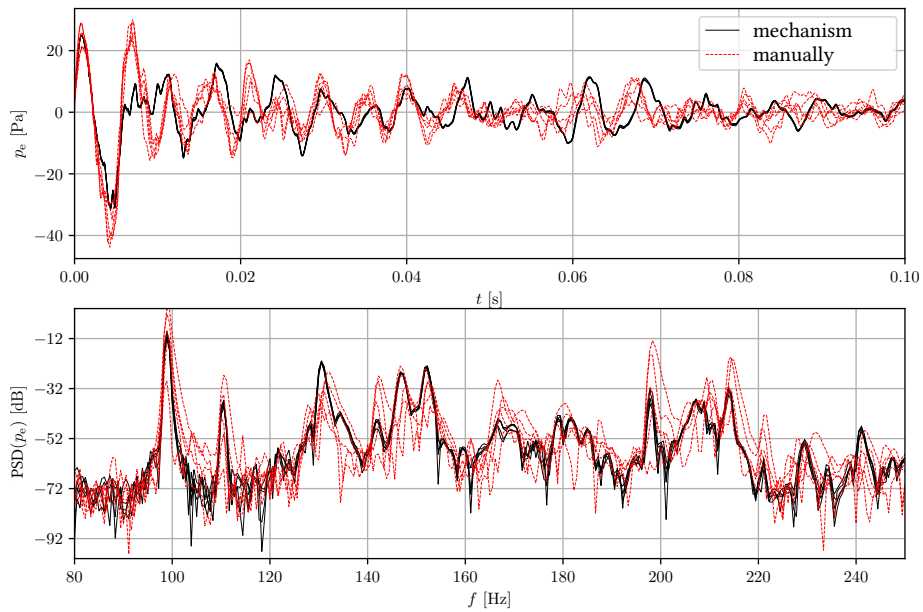


Figure 20: Testbench with a microphone as sensor, Coala as microcontroller and loudspeaker as actuator. The second microphone above the tom-tom drum is used to measure the external pressure $p_e(t)$.



(a) Principle: the drumstick that is initially held against a stop, is released and caught after one impact on the center of the tom-tom membrane.



(b) Efficiency evaluated by comparing time and frequency evolutions for 5 manual impacts vs. 5 impacts with the excitation mechanism: the temporal measurements coincide almost perfectly in the latter case.

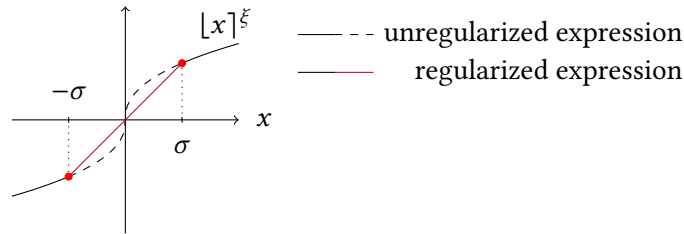
Figure 21: Reproducible excitation mechanism.

5 Evaluation

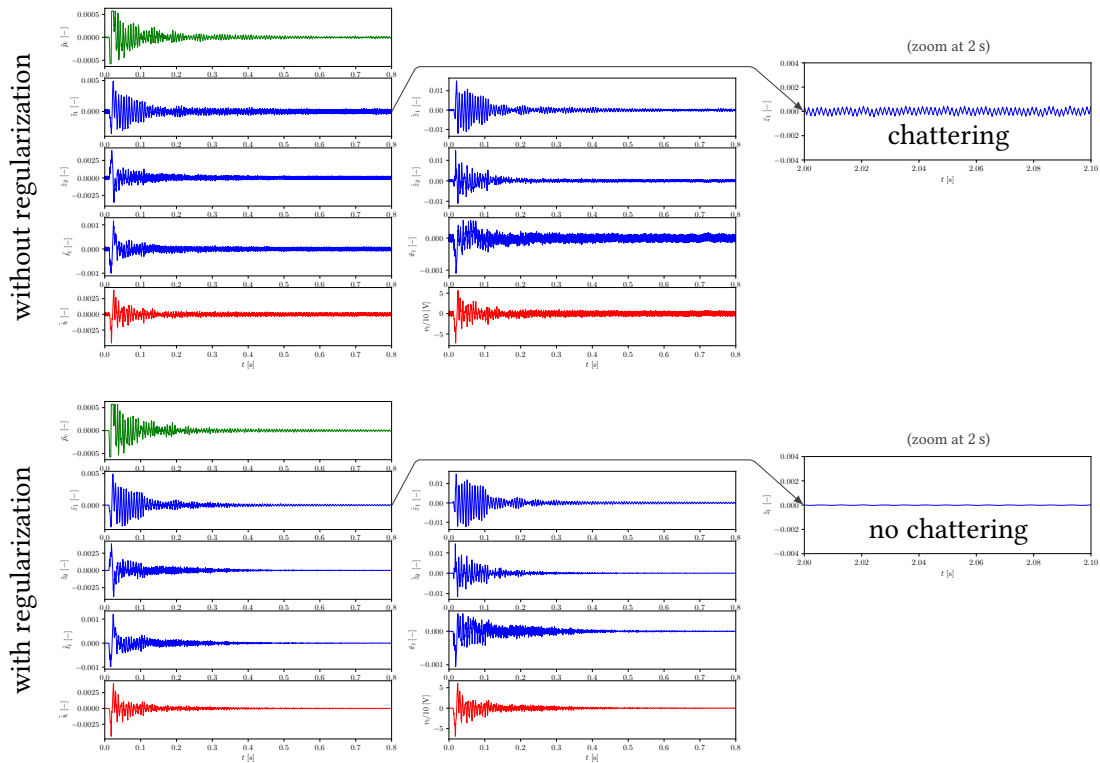
Two properties of the testbench are assessed: an evaluation of the numerical stiffness of the finite-time observer-regulator (Subsection 5.1), and an evaluation of the ability to modify the frequency of the first two axisymmetric membrane modes (Subsection 5.2).

5.1 Numerical stiffness

When testing the control loop, a high-frequency noise is noticed (Fig. 22), even when the pressure inside the cavity is very small. This chattering phenomenon is caused by the inherent stiffness [Bhat et al. 2000] of the nonlinear expression $[x]^\xi$ in the used finite-time control law (5) and finite-time observer at $x = 0$. A local softening linear interpolation¹⁷ of these expressions around 0 suffices to remove this phenomenon (Fig. 22).



(a) Regularization of the stiff expression $[x]^\xi$ present in control law and observer



(b) Effect on the internal variables of the Coala: pressure measurement in green, state of the observer in blue ($N = 2$ modes and loudspeaker), calculated current/tension control law in red. They exhibit a chattering phenomenon (the case of $\tilde{z}_1(t)$ being shown well after an impact), that is removed by the regularization of the expression $[x]^\xi$. (Tildes indicate nondimensionalized versions of the respective signals, cf. [Wijnand et al. 2019; Wijnand et al. 2020].)

Figure 22: Evaluation of the numerical method.

¹⁷ The nonlinear expression $[x]^\xi$ was replaced by a local softening linear interpolation between the boundary values for the (nondimensionalized [Wijnand et al. 2019; Wijnand et al. 2020]) arguments x at $x = \pm\sigma$, with $\sigma = 10^{-5}$ (resp. 10^{-3}) for the observer (resp. controller).

5.2 Frequency shift

The testbench is placed in Ircam’s anechoic chamber¹⁸. Different sets of pole placement parameters ($k_{1,a}, k_{2,a}$) are selected (see Table 3) and for each, the resulting sound is measured thrice (Figs. 23-24). The power spectral density (PSD) shows that the controller enables to obtain frequency shifts, as compared to the uncontrolled case.

Table 3: List of used pole placement parameters: $k_{1,a}$ and $k_{2,a}$ are varied, $k_{1,b} = k_{2,b} = 0$. The corresponding frequency shift for control 6 is indicated. The other sets of pole placement parameters cannot be interpreted as a frequency shift by the used model (cf. Footnote 19).

case	$k_{1,a}$	$k_{2,a}$	f_{01} [Hz]	f_{02} [Hz]
no control	–	–	142.93	201.16
control 0	0	0	142.93	201.16
control 1	0	0.2	N/A	N/A
control 2	0	–0.12	N/A	N/A
control 3	0.125	0	N/A	N/A
control 4	–0.25	0	N/A	N/A
control 5	0.125	0.125	N/A	N/A
control 6	–0.2	–0.2	165.69 (+15.9%)	206.30 (+2.6%)
control 7	0.05	–0.05	N/A	N/A
control 8	–0.075	0.075	N/A	N/A

It is noted that the PSD does not contain the temporal evolution of the frequencies. This information can be seen in an HR-ogram, an example being given in Figs. 25-26.

Among the tested pole placement parameters (Table 3), only the control 6 can be interpreted as a frequency shift¹⁹. The PSD of this case is shown in Figure 27. However, due to the observed disparity between the measurements and the predicted frequencies that were calculated using the simplified model, it is difficult to evaluate the controller performance in achieving the control objective (a frequency shift in this case).

¹⁸ This anechoic chamber has the form of a rectangular cuboid of usable volume $5.7 \times 4.3 \times 4.2 \text{ m}^3$, whose walls are covered with triangular absorbing prisms, and has a sound level of ca. 18.5 dB SPL (A) [Carpentier et al. 2014].

¹⁹ The predicted frequency shift is obtained by performing the pole placement using Ackermann’s formula [Ackermann 1977, Eq. 13] on the state-space representation of the tom membrane subsystem with 2 modes [Wijnand 2021, §C.3.1.1] that is controlled by the cavity pressure following Eq. (6).

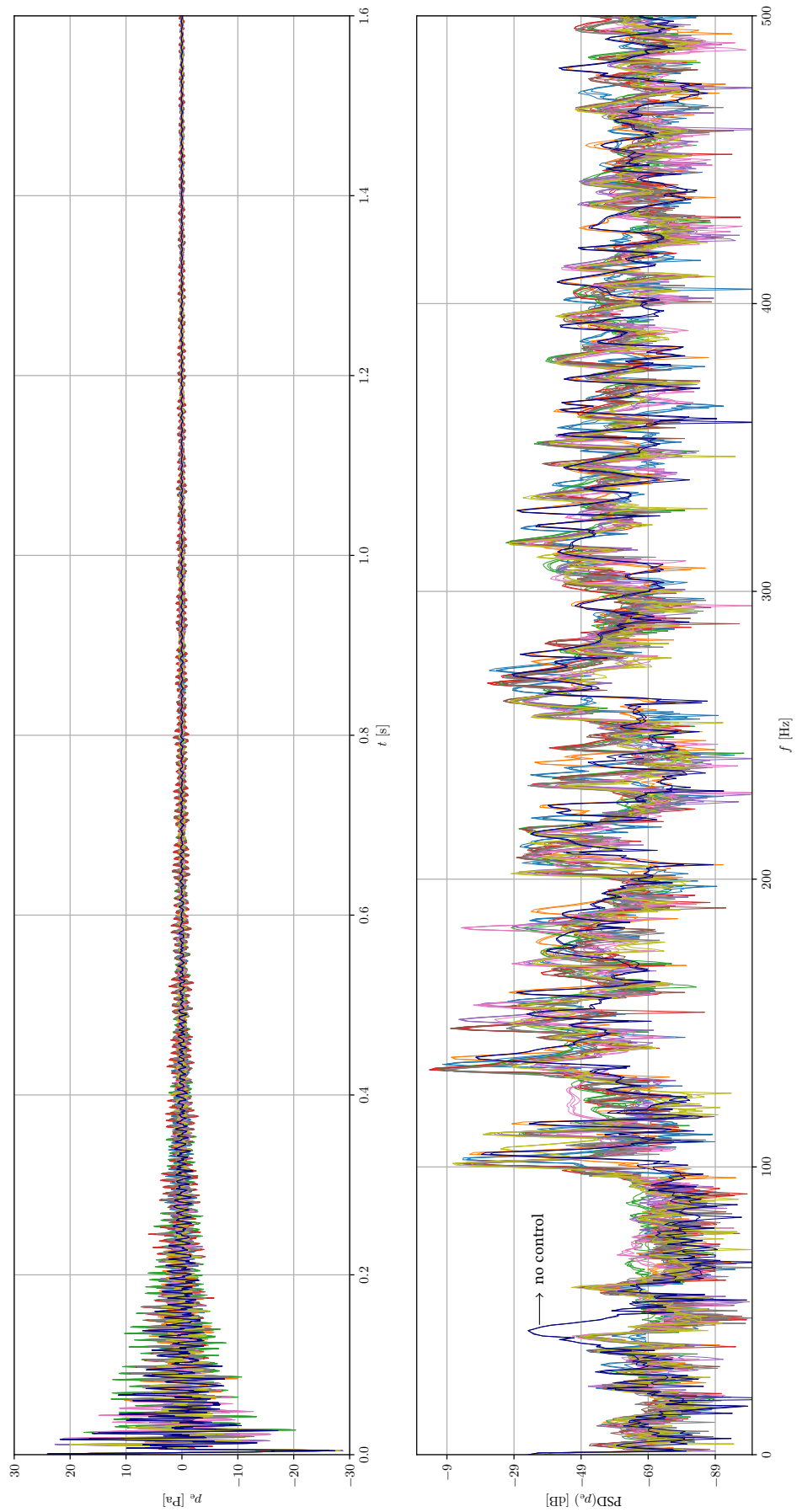


Figure 23: Power spectral density ([Welch 1967], calculated for signal durations of 1.6 s) for measurements of the pressure $p_e(t)$ obtained with different pole placement parameters (different colours). The uncontrolled case is indicated in dark blue.

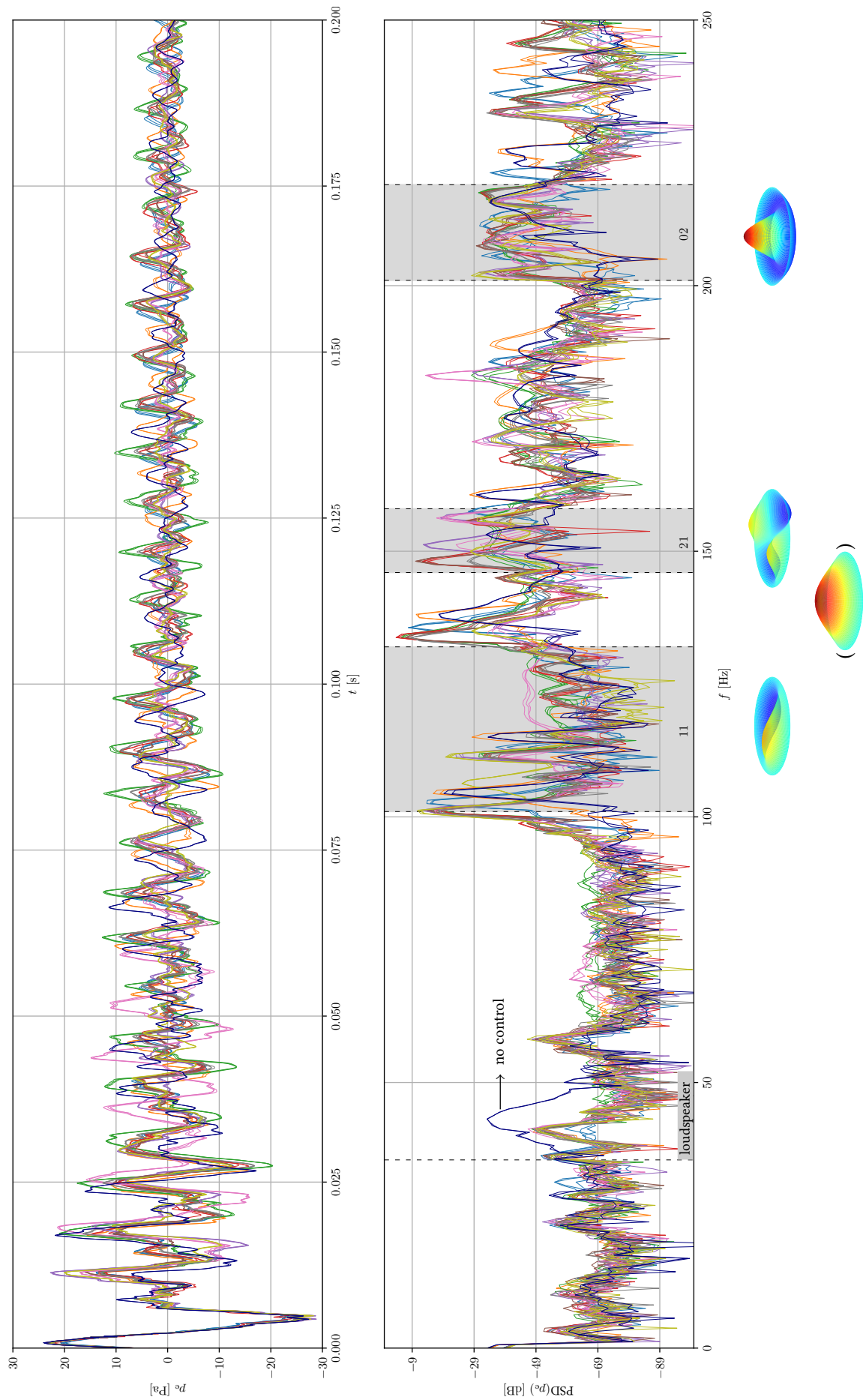


Figure 24: Detail of Figure 23. Frequency bands for the experimentally observed Chladni figures (cf. Figs. 15-16) are indicated in gray.

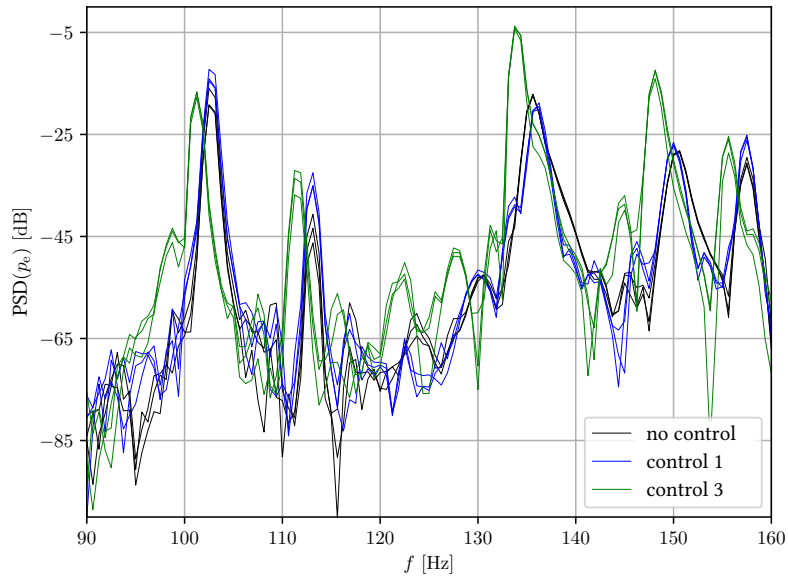


Figure 25: Detail of the PSD for the uncontrolled case and two controlled cases (control 1 and control 3, cf. Table 3).

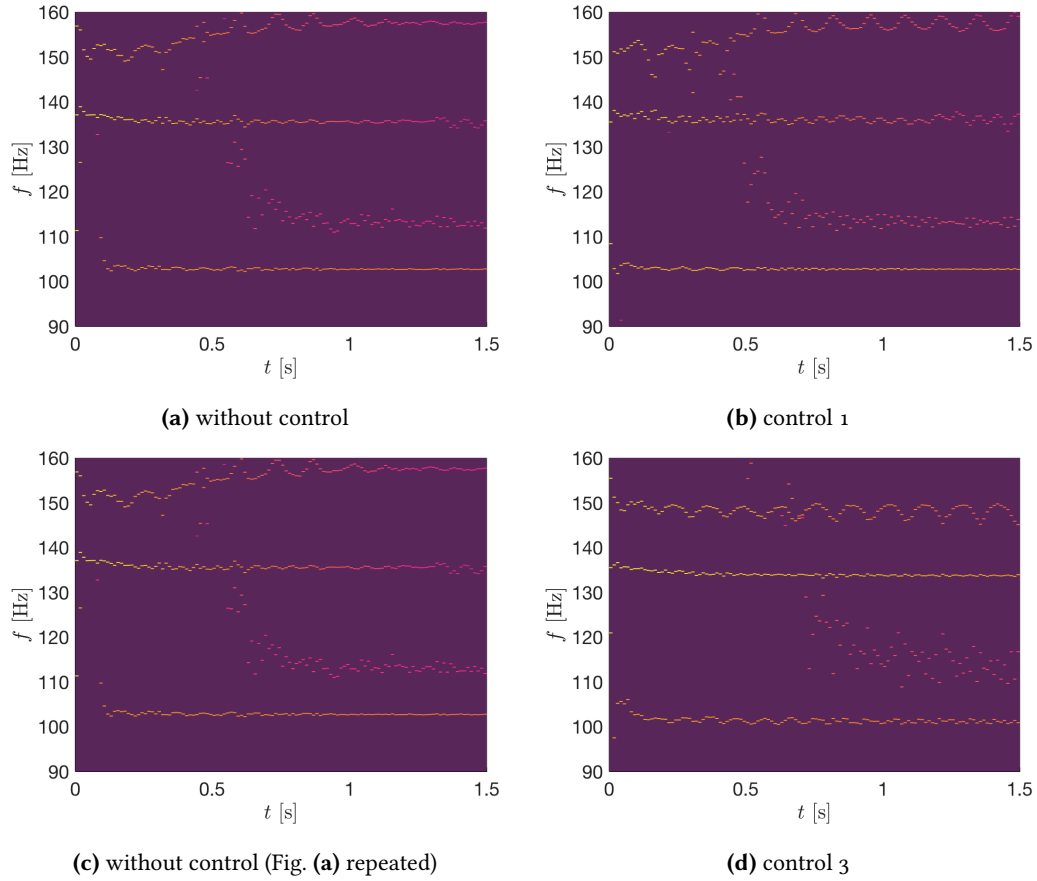


Figure 26: Details of the HR-ograms corresponding to Fig. 25.

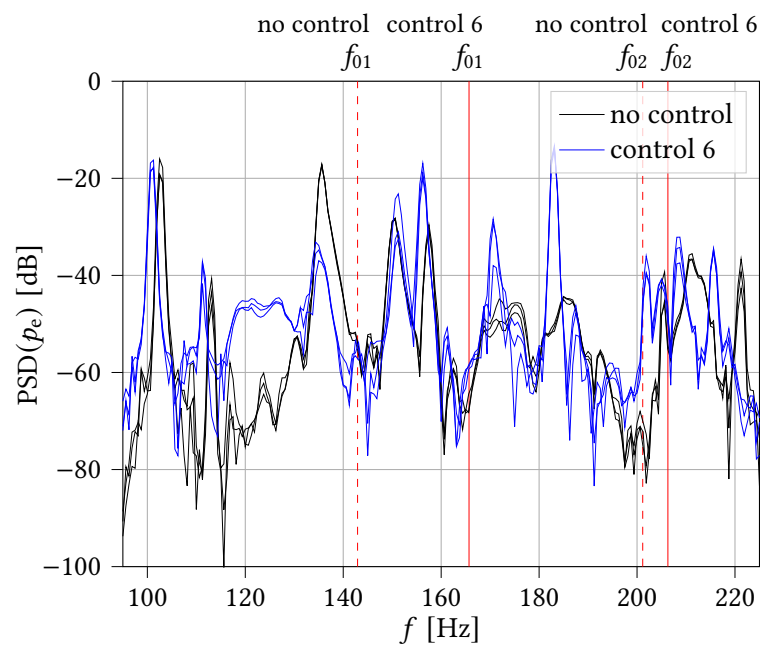


Figure 27: Detail of the PSD for the uncontrolled case and a controlled case (control 6). One observes a disparity between the obtained frequency peaks and the frequencies f_{01} and f_{02} that were calculated using the model (cf. Table 3).

6 Conclusion and perspectives

The experimental implementation of a previously derived finite-time observer-regulator for a tom-tom drum augmented with a loudspeaker was discussed.

Firstly, a chattering phenomenon was observed, caused by the stiffness of the used control law. This was removed by a local softening linear interpolation of the non Lipschitz continuous expressions.

Secondly, it was shown that the proposed control architecture enables to modify frequencies of the tom-tom membrane, while sensor and actuator are located outside the tom membrane domain. However, because of the disparity between model and measurements, it is difficult to quantify the controller performance in achieving a prescribed frequency shift.

In order to improve the performance of the proposed finite-time observer-regulator structure, the used model could be refined. The most important contribution would be to include the neglected time delays that exist between sensor, membrane and actuator (Fig. 28). Furthermore, the cavity and radiation dynamics could be included, and the tuning of the membrane studied more thoroughly. Finally, the robustness of the proposed finite-time controller against bad model parameter estimation could be improved by a passivity-based design (cf. [Wijnand et al. 2018]).

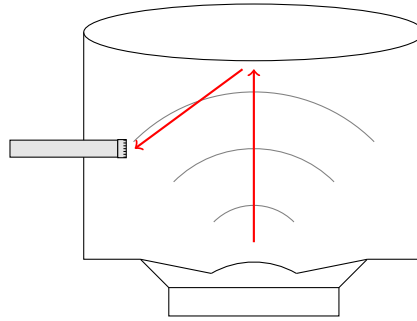


Figure 28: Propagation of sound waves inside the cavity, actuator (loudspeaker) and sensor (microphone) located outside the tom membrane domain.

Acknowledgements

Brigitte d'Andréa-Novel and Marc Wijnand were supported by ANR project Finite4SoS (ANR 15 CE23 0007). The authors thank Emmanuel Fléty, Tristan Lebrun, Robert Piéchaud and Arnaud Recher for technical support.

This work is dedicated to the memory of Simon Benacchio.

References

- Ackermann, J. (1977). “Entwurf durch Polvorgabe [Design by pole placement]”. *at-Automatisierungstechnik* 25.1-12, 173–179 & 209–215. DOI: [10.1524/auto.1977.25.112.173](https://doi.org/10.1524/auto.1977.25.112.173)
- Anderson, C. A. (1978). “The acoustics of timpani: an analysis of vibrating circular membranes”. Master’s thesis. Northern Illinois University
- Badeau, R. (2005). “Méthodes à haute résolution pour l’estimation et le suivi de sinusoïdes modulées. Application aux signaux de musique”. PhD thesis. Télécom ParisTech. URL: <https://hal.science/tel-00009321v1/document>
- Badeau, R., B. David, and G. Richard (2006). “A new perturbation analysis for signal enumeration in rotational invariance techniques”. *IEEE Transactions on Signal Processing* 54.2, pp. 450–458. DOI: [10.1109/tsp.2005.861899](https://doi.org/10.1109/tsp.2005.861899)
- Bader, R. (2016). “Finite-Difference model of mode shape changes of the Myanmar *pat wain* drum circle using tuning paste”. *172nd Meeting of the Acoustical Society of America*. Vol. 29. 1. Acoustical Society of America, pp. 3086–3094. DOI: [10.1121/2.0000450](https://doi.org/10.1121/2.0000450)
- Benacchio, S., B. Chomette, A. Mamou-Mani, and V. Finel (2015). “Mode tuning of a simplified string instrument using time-dimensionless state-derivative control”. *Journal of sound and vibration* 334, pp. 178–189. DOI: [10.1016/j.jsv.2014.09.003](https://doi.org/10.1016/j.jsv.2014.09.003)
- Benacchio, S., A. Mamou-Mani, B. Chomette, and V. Finel (2016). “Active control and sound synthesis—two different ways to investigate the influence of the modal parameters of a guitar on its sound”. *The Journal of the Acoustical Society of America* 139.3, pp. 1411–1419. DOI: [10.1121/1.4944572](https://doi.org/10.1121/1.4944572)
- Berdahl, E. and J. O. Smith III (2007). “Inducing unusual dynamics in acoustic musical instruments”. *2007 IEEE International Conference on Control Applications*. IEEE, pp. 1336–1341. DOI: [10.1109/cca.2007.4389421](https://doi.org/10.1109/cca.2007.4389421)
- Berdahl, E., J. O. Smith III, and A. Freed (2006). “Active damping of a vibrating string”. *2006 International Symposium on Active Control of Sound and Vibration*
- Berg, R. E. and D. G. Stork (2005). *The Physics of Sound*. 3rd edition. Pearson. ISBN: 9780131457898
- Bernuau, E., W. Perruquetti, D. Efimov, and E. Moulay (2015). “Robust finite-time output feedback stabilisation of the double integrator”. *International Journal of Control* 88.3, pp. 451–460. DOI: [10.1080/00207179.2014.956340](https://doi.org/10.1080/00207179.2014.956340)
- Bertsch, M. (2001). “Vibration patterns and sound analysis of the Viennese Timpani”. *International Symposium on Musical Acoustics (ISMA), Perugia, Italy*, pp. 281–284
- Besnainou, C. (1999). “Transforming the voice of musical instruments by active control of the sound radiation”. *INTER-NOISE and NOISE-CON Congress and Conference Proceedings*. 5. Institute of Noise Control Engineering, pp. 1317–1321
- Besnainou, C. (2006). “Comment changer la voix des instruments de musique”. *Rencontres Musicales Pluridisciplinaires, GRAME, Lyon*
- Bhat, S. P. and D. S. Bernstein (2000). “Finite-time stability of continuous autonomous systems”. *SIAM Journal on Control and Optimization* 38.3, pp. 751–766. DOI: [10.1137/s0363012997321358](https://doi.org/10.1137/s0363012997321358)
- Bork, I. (1983). *Entwicklung von akustischen Optimierungsverfahren für Stabspiele und Membraninstrumente*. PTB Report, Projekt 5267, Braunschweig
- Boutin, H., C. Besnainou, and J.-D. Polack (2015). “Modifying the resonances of a xylophone bar using active control”. *Acta Acustica united with Acustica* 101.2, pp. 408–420. DOI: [10.3813/aaa.918836](https://doi.org/10.3813/aaa.918836)
- Bouvier, D. (2018). “Identification de systèmes non linéaires représentés en séries de Volterra: applications aux systèmes sonores”. PhD thesis. Sorbonne Université/Université Pierre et Marie Curie-Paris VI. URL: <https://theses.hal.science/tel-01992229v2/document>
- Branch, M. A., T. F. Coleman, and Y. Li (1999). “A subspace, interior, and conjugate gradient method for large-scale bound-constrained minimization problems”. *SIAM Journal on Scientific Computing* 21.1, pp. 1–23. DOI: [10.1137/s1064827595289108](https://doi.org/10.1137/s1064827595289108)
- Brunet, P. (2014). “Nonlinear system modeling and identification of loudspeakers”. PhD thesis. Northeastern University Boston. DOI: [10.17760/d20004964](https://doi.org/10.17760/d20004964)
- Cahoon, D. E. (1970). “Frequency-Time Analysis of the Bass Drum Sound”. Master’s thesis. Brigham Young University, Provo, Utah

- Carpentier, T., H. Bahu, M. Noisternig, and O. Warusfel (2014). “Measurement of a head-related transfer function database with high spatial resolution”. *7th Forum Acusticum (EAA)*
- Chaigne, A. (2000). “Détermination expérimentale de la tension d’une peau de timbale”. *Actes du 5ème Congrès Français d’Acoustique*, pp. 251–253
- Chaigne, A. and V. Doutaut (1997). “Numerical simulations of xylophones. I. Time-domain modeling of the vibrating bars”. *The Journal of the Acoustical Society of America* 101.1, pp. 539–557. DOI: [10.1121/1.418117](https://doi.org/10.1121/1.418117)
- Chaigne, A. and J. Kergomard (2016). *Acoustics of musical instruments*. Springer. ISBN: 9781493936779. DOI: [10.1007/978-1-4939-3679-3](https://doi.org/10.1007/978-1-4939-3679-3)
- Chladni, E. F. F. (1787). *Entdeckungen über die Theorie des Klanges*. Weidmanns Erben und Reich, Leipzig. DOI: [10.14711/spcol/b495277](https://doi.org/10.14711/spcol/b495277)
- Christian, R. S., R. E. Davis, A. Tubis, C. A. Anderson, R. I. Mills, and T. D. Rossing (1984). “Effects of air loading on timpani membrane vibrations”. *The Journal of the Acoustical Society of America* 76.5, pp. 1336–1345. DOI: [10.1121/1.391449](https://doi.org/10.1121/1.391449)
- Dahl, S. (1997). “Spectral changes in the tom-tom related to striking force”. *Music and Hearing - Quarterly Progress and Status Report* 38.1, pp. 59–65
- Elliott, S. (2000). *Signal processing for active control*. Elsevier. ISBN: 9780122370854
- Elliott, S. J. and P. A. Nelson (1993). “Active noise control”. *IEEE signal processing magazine* 10.4, pp. 12–35. DOI: [10.1109/79.248551](https://doi.org/10.1109/79.248551)
- Fleischer, H. (2005). *Beiträge zur Vibro- und Psychoakustik: Vibroakustische Untersuchungen an Paukenfellen*. ISSN: 1430-936X. Universität der Bundeswehr München
- Fletcher, H. and I. G. Bassett (1978). “Some experiments with the bass drum”. *The Journal of the Acoustical Society of America* 64.6, pp. 1570–1576. DOI: [10.1121/1.382140](https://doi.org/10.1121/1.382140)
- Fletcher, N. H. and T. D. Rossing (2012). *The physics of musical instruments*. Springer Science & Business Media
- Fuller, C. C., S. Elliott, and P. A. Nelson (1996). *Active control of vibration*. Academic Press. ISBN: 978-0-12-269440-0. DOI: [10.1016/B978-0-12-269440-0.X5000-6](https://doi.org/10.1016/B978-0-12-269440-0.X5000-6)
- Graff, K. F. (2012). *Wave motion in elastic solids*. Courier Corporation. ISBN: 9780486139579
- Gregorio, J. and Y. Kim (2018). “Augmentation of acoustic drums using electromagnetic actuation and wireless control”. *Journal of the Audio Engineering Society* 66.4, pp. 202–210. DOI: [10.17743/jaes.2018.0008](https://doi.org/10.17743/jaes.2018.0008)
- Haimo, V. T. (1986). “Finite time controllers”. *SIAM Journal on Control and Optimization* 24.4, pp. 760–770. DOI: [10.1137/0324047](https://doi.org/10.1137/0324047)
- Harms, B. (2008). “The World of Historical Timpani”. *Early Music America* 14.2, pp. 29–36
- Hélie, T. and C. Picasso (2017). “The Snail: a real-time software application to visualize sounds”. *International Conference on Digital Audio Effects (DAFx)*. Vol. 20, pp. 443–450
- Jossic, M. (2017). “Contrôle actif et non-linéarités géométriques : le cas du gong xiaoluo”. PhD thesis. Université Pierre et Marie Curie, Paris. URL: <https://theses.hal.science/tel-01901105v1/document>
- Jossic, M., A. Mamou-Mani, B. Chomette, D. Roze, F. Ollivier, and C. Josserand (2017). “Modal active control of Chinese gongs”. *The Journal of the Acoustical Society of America* 141.6, pp. 4567–4578. DOI: [10.1121/1.4985108](https://doi.org/10.1121/1.4985108)
- Kinsler, L. E., A. R. Frey, A. B. Coppens, and J. V. Sanders (1999). *Fundamentals of acoustics*. 4th. Wiley. ISBN: 9780471847892
- Klippel, W. and U. Seidel (2001). “Fast and accurate measurement of linear transducer parameters”. *110th AES Convention, Amsterdam*.
- Knudsen, M. H., J. G. Jensen, V. Julskjaer, and P. Rubak (1989). “Determination of loudspeaker driver parameters using a system identification technique”. *Journal of the Audio Engineering Society* 37.9, pp. 700–708
- Krump, G. (1997). “Zur Temperaturabhängigkeit von Lautsprecherparametern”. *Presentation at DAGA-97, Kiel, Allemagne*
- Lagrange, M., R. Badeau, B. David, N. Bertin, J. Echeveste, O. Derrien, S. Marchand, and L. Daudet (2010). “The DESAM toolbox: spectral analysis of musical audio”. *International Conference on Digital Audio Effects (DAFx), Graz*

- Laroche, J. (1993). “The use of the matrix pencil method for the spectrum analysis of musical signals”. *The Journal of the Acoustical Society of America* 94.4, pp. 1958–1965. DOI: [10.1121/1.407519](https://doi.org/10.1121/1.407519)
- Le Carrou, J.-L., F. Gautier, and R. Badeau (2009). “Sympathetic string modes in the concert harp”. *Acta Acustica united with Acustica* 95.4, pp. 744–752. DOI: [10.3813/aaa.918202](https://doi.org/10.3813/aaa.918202)
- Lebrun, T. (2019). “Modélisation multi-physique passive, identification, simulation, correction et asservissement de haut-parleur sur des comportements cibles”. PhD thesis. Sorbonne Université
- Lupone, M. and L. Seno (2005). “Gran cassa and the adaptive instrument feed-drum”. *International Symposium on Computer Music Modeling and Retrieval*. Springer, pp. 149–163. DOI: [10.1007/11751069_14](https://doi.org/10.1007/11751069_14)
- Maugeais, S. (2014). “How to apply a plaster on a drum to make it harmonic”. *International Symposium on Musical Acoustics, ISMA*
- Meurisse, T., A. Mamou-Mani, S. Benacchio, B. Chomette, V. Finel, D. B. Sharp, and R. Caussé (2015a). “Experimental Demonstration of the Modification of the Resonances of a Simplified Self-Sustained Wind Instrument Through Modal Active Control”. *Acta Acustica united with Acustica* 101.3, pp. 581–593. DOI: [10.3813/aaa.918854](https://doi.org/10.3813/aaa.918854)
- Meurisse, T., A. Mamou-Mani, R. Caussé, B. Sluchin, and D. B. Sharp (2015b). “An active mute for the trombone”. *The Journal of the Acoustical Society of America* 138.6, pp. 3539–3548. DOI: [10.1121/1.4936901](https://doi.org/10.1121/1.4936901)
- Michels, U. (1988). *Guide illustré de la musique – Volume I*. Fayard. ISBN: 9782213021898
- Morse, P. M. (1995). *Vibration and sound*. American Society of Acoustics
- Moulay, E. and W. Perruquetti (2006). “Finite time stability and stabilization of a class of continuous systems”. *Journal of Mathematical analysis and applications* 323.2, pp. 1430–1443. DOI: [10.1016/j.jmaa.2005.11.046](https://doi.org/10.1016/j.jmaa.2005.11.046)
- Neubauer, P., J. Tschesche, J. Bös, T. Melz, and H. Hanselka (2018). “An active-system approach for eliminating the wolf note on a cello”. *The Journal of the Acoustical Society of America* 143.5, pp. 2965–2974. DOI: [10.1121/1.5037467](https://doi.org/10.1121/1.5037467)
- Pedersen, B. R. and P. Rubak (2007). “Online identification of linear loudspeakers parameters”. *Audio Engineering Society Convention 122*. Audio Engineering Society
- Perruquetti, W., T. Floquet, and E. Moulay (2008). “Finite-time observers: application to secure communication”. *IEEE Transactions on Automatic Control* 53.1, pp. 356–360. DOI: [10.1109/tac.2007.914264](https://doi.org/10.1109/tac.2007.914264)
- Piéchaud, R. (2014). “A lightweight C++ framework for real time active control”. *Real time Linux workshop*
- Raman, C. V. (1934). “The Indian musical drums”. *Proceedings of the Indian Academy of Sciences-Section A*. Vol. 1. 3. Springer, pp. 179–188. DOI: [10.1007/bf03035705](https://doi.org/10.1007/bf03035705)
- Rector, D. and S. Topel (2014). “EMdrum: An Electromagnetically Actuated Drum”. *Proc. of NIME*, pp. 395–398
- Rhaouti, L., A. Chaigne, and P. Joly (1999). “Time-domain modeling and numerical simulation of a kettledrum”. *The Journal of the Acoustical Society of America* 105.6, pp. 3545–3562. DOI: [10.1121/1.424679](https://doi.org/10.1121/1.424679)
- Richardson, P. G. M. (2010). “Acoustic analysis and tuning of cylindrical membranophones”. PhD thesis. Anglia Ruskin University
- Richardson, P. G. M. and E. R. Toulson (2010). “Clearing the drumhead by acoustic analysis method”. *Proceedings of the Institute on Acoustics, Reproduced Sound Conference, Cardiff, Wales, UK*
- Rollow IV, J. D. T. (2003). “Active Control of Spectral Detail Radiated by an air-loaded impacted membrane”. PhD thesis. The Pennsylvania State University
- Rose, C. D. (1978). “A New Drumhead Design: An Analysis of the Nonlinear Behavior of a Compound Membrane”. PhD thesis. Northern Illinois University
- Rossing, T. D. (1982a). “Nonlinear Effects in Percussion Instruments”. *Percussive Notes Research Edition* 3, pp. 68–72
- Rossing, T. D. (1982b). “The physics of kettledrums”. *Scientific American* 247.5, pp. 172–179. DOI: [10.1038/scientificamerican1182-172](https://doi.org/10.1038/scientificamerican1182-172)

- Rossing, T. D., I. Bork, H. Zhao, and D. O. Fystrom (1992). “Acoustics of snare drums”. *The Journal of the Acoustical Society of America* 92.1, pp. 84–94. DOI: [10.1121/1.404080](https://doi.org/10.1121/1.404080)
- Roy, R., A. Paulraj, and T. Kailath (1986). “ESPRIT—A subspace rotation approach to estimation of parameters of cisoids in noise”. *IEEE transactions on acoustics, speech, and signal processing* 34.5, pp. 1340–1342. DOI: [10.1109/tassp.1986.1164935](https://doi.org/10.1109/tassp.1986.1164935)
- Samejima, T. and R. Fukuda (2016). “Vibration analysis of a musical drum head under nonuniform density and tension using a spectral method”. *Acoustical Science and Technology* 37.6, pp. 295–302. DOI: [10.1250/ast.37.295](https://doi.org/10.1250/ast.37.295)
- Sathej, G. and R. Adhikari (2009). “The eigenspectra of Indian musical drums”. *The Journal of the Acoustical Society of America* 125.2, pp. 831–838. DOI: [10.1121/1.3058632](https://doi.org/10.1121/1.3058632)
- Small, R. H. (1972). “Closed-box loudspeaker systems-part 1: Analysis”. *Journal of the Audio Engineering Society* 20.10, pp. 798–808
- Small, R. H. (1973). “Closed-box loudspeaker systems-part 2: Synthesis”. *Journal of the Audio Engineering Society* 21.1, pp. 11–18
- Solomon, S. Z. (2016). *How to write for Percussion: a comprehensive guide to percussion composition*. Oxford University Press. ISBN: 9780199920365
- Sullivan, D. L. (1997). “Accurate frequency tracking of timpani spectral lines”. *The Journal of the Acoustical Society of America* 101.1, pp. 530–538. DOI: [10.1121/1.418116](https://doi.org/10.1121/1.418116)
- Thiele, N. (1971a). “Loudspeakers in vented boxes: Part 1”. *Journal of the Audio Engineering Society* 19.5, pp. 382–392
- Thiele, N. (1971b). “Loudspeakers in vented boxes: Part 2”. *Journal of the Audio Engineering Society* 19.6, pp. 471–483
- Torin, A. and M. Newton (2014). “Nonlinear effects in drum membranes”. *Proceedings of the International Symposium on Musical Acoustics*, pp. 107–112
- Van Walstijn, M. and P. Rebelo (2005). “The prosthetic conga: Towards an actively controlled hybrid musical instrument”. *ICMC*. Citeseer
- Von Hornbostel, E. M. and C. Sachs (1914). “Systematik der Musikinstrumente. Ein Versuch”. *Zeitschrift für Ethnologie* 46.H. 4/5, pp. 553–590
- Welch, P. (1967). “The use of fast Fourier transform for the estimation of power spectra: a method based on time averaging over short, modified periodograms”. *IEEE Transactions on audio and electroacoustics* 15.2, pp. 70–73. DOI: [10.1109/tau.1967.1161901](https://doi.org/10.1109/tau.1967.1161901)
- Wijnand, M. (2021). “Contrôle en temps fini de systèmes vibratoires hybrides couplant équations aux dérivées partielles et équations aux dérivées ordinaires : les cas du tom et du câble pesant”. PhD thesis. Sorbonne Université, Paris, France. URL: <https://theses.hal.science/tel-03722379/document>
- Wijnand, M., B. d’Andréa-Novel, B. Fabre, T. Hélie, L. Rosier, and D. Roze (2019). “Active control of the axisymmetric vibration modes of a tom-tom drum”. *2019 IEEE 58th Conference on Decision and Control (CDC)*. IEEE, pp. 6887–6892. DOI: [10.1109/cdc40024.2019.9029960](https://doi.org/10.1109/cdc40024.2019.9029960)
- Wijnand, M., B. d’Andréa-Novel, T. Hélie, and D. Roze (2018). “Contrôle des vibrations d’un oscillateur passif : stabilisation en temps fini et par remodelage d’énergie”. *Congrès Français d’Acoustique, Le Havre*
- Wijnand, M., B. d’Andréa-Novel, T. Hélie, and D. Roze (2020). “Active control of the axisymmetric vibration modes of a tom-tom drum using a modal-based observer-regulator”. *EAA e-Forum Acusticum*, pp. 639–646. DOI: [10.48465/fa.2020.0439](https://doi.org/10.48465/fa.2020.0439)
- Wijnand, M., B. d’Andréa-Novel, T. Hélie, and D. Roze (2023). “Experimental implementation of a finite-time controller for the axisymmetric vibration modes of a tom-tom drum”. *Forum Acusticum, Torino*
- Wijnand, M., T. Hélie, and D. Roze (2022). “Finite-time tracking control of a nonlinear string to reference dynamics”. *10th European Nonlinear Dynamics Conference (ENOC 2020+2)*, Lyon, France. DOI: [10.1007/978-3-030-34747-5_3](https://doi.org/10.1007/978-3-030-34747-5_3)
- Williams, P. and D. Overholt (2020). “Design and evaluation of a digitally active drum”. *Personal and Ubiquitous Computing*, pp. 783–795. DOI: [10.1007/s00779-020-01391-6](https://doi.org/10.1007/s00779-020-01391-6)
- Worland, R. (2010). “Normal modes of a circular drumhead under non-uniform tension”. *The Journal of the Acoustical Society of America* 127.1, pp. 525–533. DOI: [10.1121/1.3268605](https://doi.org/10.1121/1.3268605)

Worland, R. (2011). “Chladni patterns on drumheads: a “physics of music” experiment”. *The Physics Teacher* 49.1, pp. 24–27. DOI: [10.1119/1.3527750](https://doi.org/10.1119/1.3527750)

A Appendix: Experimental devices

The used devices are listed in Tables 4-5. Excerpts from the datasheets are shown in [Wijnand 2021, Appendix D.4].

Table 4: List of devices used for the identification.

loudspeaker identification	power amplifier	Newtons4th Ltd LPA05
	current sensor	Newtons4th Ltd HF003
	laser sensor	Keyence LK-H050
membrane tuning	microphone	Bruel & Kjaer 4190
	microphone conditioner	Nexus 2690
	impact hammer	Dytran 5800SL
	impact hammer amplifier	MMF M32
membrane identification	function generator	TTi TG2000
	shaker	Bruel & Kjaer 4810
	shaker amplifier	ILP Electronics US1 Power slave
overall	acquisition card	National Instruments 9234

Table 5: List of devices used for the testbench.

microphone (in cavity)	Bruel & Kjaer 4939
microphone (above tom)	Bruel & Kjaer 4191
microphone conditioner	Nexus 2690
microcontroller	Coala (v1) "Alto" [Piéchaud 2014]
loudspeaker amplifier	Newtons4th Ltd LPA05
acquisition card	National Instruments 9234

B Appendix: Chladni figures

Further obtained Chladni figures are shown in Fig. 29.

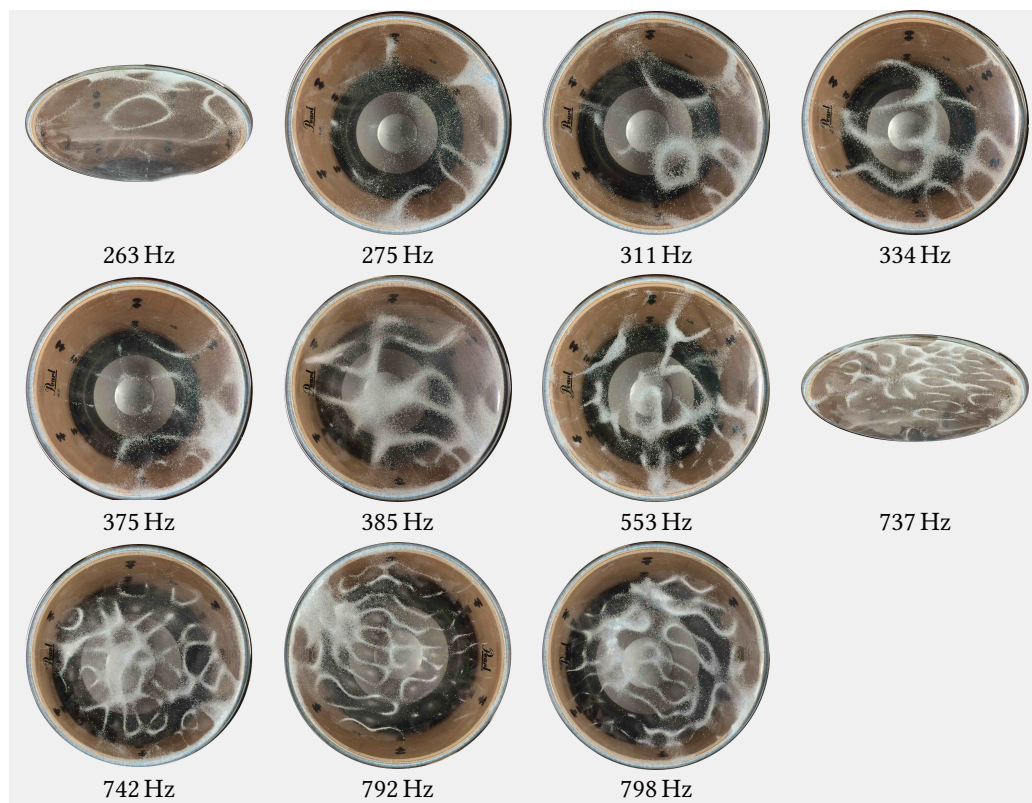


Figure 29: Some Chladni figures at higher frequencies than those shown in Fig. 15.